DFN Analysis to Quantify the Reliability of Borehole Derived Volumetric Intensity

by

Pedro Pablo Ojeda Selame

BSE., The Pontificia Universidad Católica de Chile, 2008

A THESIS SUBMITTED IN PARTIAL FULFILLMENT OF

THE REQUIREMENTS FOR THE DEGREE OF

MASTER OF APPLIED SCIENCE

in

THE FACULTY OF GRADUATE AND POSTDOCTORAL STUDIES

(Mining Engineering)

THE UNIVERSITY OF BRITISH COLUMBIA

(Vancouver)

August 2022

The following individuals certify that they have read, and recommend to the Faculty of Graduate and Postdoctoral Studies for acceptance, the thesis entitled:

DFN Analysis to Quantify the Reliability of Borehole Derived Volumetric Intensity

submitted by Pedro Pablo Ojeda Selame in partial fulfilment of the requirements for

the degree of Master of Applied Science

in Mining Engineering

Examining Committee:

Davide Elmo, Professor, Mining Engineering, UBC
Supervisor

Bern Klein, Professor, Mining Engineering, UBC
Supervisory Committee Member

Abstract

Volumetric fracture intensity (P_{32}) is a parameter that plays a major role in the mechanical and hydraulic behaviour of rock masses. Although it is not possible to measure P_{32} directly using current technologies, P_{32} can be estimated from borehole and surface data using either simulation or analytical solutions.

In this thesis we use Discrete Fracture Network (DFN) models to addresses the problem of estimating P_{32} using information from boreholes (1D data), and we also investigate the problem of quantify the uncertainty range of the calculated P_{32}. Based on the comparison between actual P_{32} and the intensity sampled using synthetic boreholes, we propose a new methodology to estimate P_{32} variability from linear intensity. This methodology can be useful to quantify and understand the expected variability of P_{32} values of a project when linear intensity is the only information available.

It is common practice, when calculating P_{32} based on Terzaghi Weight (1965), to use drill run lengths, and limit the minimum angle between the borehole and the intersected fractures. The analysis presented in this thesis indicated that limiting the minimum angle of intersection would result in an underestimation of the calculated P_{32}. Additionally, the size of the interval has a great impact on the variability of the calculated P_{32}. To account for that we propose a methodology to calculate P_{32} using variable lengths, depending on the angle between the fractures and the borehole. This methodology allows to capture the spatial variation in intensity and at the same time it avoids

the artificial increasing or decreasing of the intensity sampled along borehole intervals. This can be useful when the interval intensity is used as input for interpolating P_{32} values in block models.

Finally, the research has addressed another fundamental issue, that is the impact of boundary effects in DFN models. The results confirmed that DFN models do present boundary effects with respect to the modelled fracture intensity and that these boundary effects are dependent on the size of the generation box in relation to the volume of interest and the size of the fractures.

Lay Summary

Volumetric fracture intensity, defined as the area of fractures per unit of volume, is an important parameter that plays a major role in the mechanical and hydraulic properties of rock masses. The main problem with determining the volumetric intensity is that this can not be measured directly from the rock mass. In practice, volumetric intensity is calculated from borehole data or surface mapping, using either simulation or mathematical solutions.

Using Discrete Fracture Network (DFN) models, this thesis investigates the relationship between volumetric intensity and borehole intensity and then proposes a methodology to mitigate DFN boundary effects, a methodology to quantify the intensity variability, and finally a methodology to calculate volumetric intensity from borehole data. The main advantage of the methodology proposed to calculate volumetric intensity, is that it is possible to capture the spatial variation in intensity without increasing artificially the variability of the intensity calculated in the borehole intervals.

Preface

This thesis is an original and independent, unpublished, work completed by the author, P. Ojeda.

Table of Contents

List of Tables

List of Figures

Acknowledgements

I would like to express my gratitude to my research supervisor Dr. Davide Elmo who has provided support, valuable technical knowledge, encouragement, and guidance through this process. Thanks to my colleagues for providing valuable advice and good ideas. Special thanks to Dr. Steve Rogers who help me to get a job in Canada and whose encouragement help me to pursue this degree.

I would also like to thank Golder Associates Ltd. for providing a job in Canada for the duration of my studies and for providing a license for the code FracMan used in the development of this thesis.

Chapter 1: Introduction

1.1 Background

A key component of understanding the behaviour of a rock mass is the characterization of discontinuities (i.e., structural features such as joints, bedding planes, faults, shear zones, etc.). Discontinuities in a rock mass are usually described as an assemblage rather than individually (Dershowitz, 1988), using specific properties, namely discontinuity orientation, size, shape, spatial location, and intensity.

The necessity of modelling discontinuities explicitly, for different engineering and geological applications, has led to an increasing use of the Discrete Fracture Network (DFN) approach, both as a stand-alone tool or integrated within more complex geomechanical models (Elmo, 2014). Note that the term fracture is herein applied in a broad context to refer to a variety of discontinuities at different scales (faults, joints, veins, etc.).

The advantage of DFN models is that is possible to generate realistic assemblages of fractures in three-dimension by using statistical distributions. The quality of a DFN and its representativity of the actual structural conditions depend both on the quality of the field data and on the techniques used to transform the field data into input for the DFN models.

One of the most important inputs for DFN analysis is fracture intensity, which can be expressed in various ways: i) the total sum of fracture surface area per unit of volume, P_{32}; ii) the total sum of fracture length per unit area, P_{21}; and iii) the total number of fractures per unit length, P_{10}.

In recent years DFN models have been used to demonstrate the role that P_{32} intensity plays on controlling a number of rock mass properties critical to caving operations (Rogers et al., 2015). Although it is not possible to measure P_{32} directly using current technologies, P_{32} can be estimated from borehole and surface data using either simulation or analytical solutions.

1.2 Research Objectives

In this thesis we use Discrete Fracture Network (DFN) models to addresses the problem of estimating P_{32} using information from boreholes (1D data), and we also investigate the problem of quantify the uncertainty range of the calculated P_{32}. Based on the comparison between actual P_{32} and the intensity sampled using synthetic boreholes, we propose a new methodology to estimate P_{32} variability from linear intensity. This methodology can be useful to quantify and understand the expected variability of P_{32} values of a project when linear intensity is the only information available.

The research has addressed the following research objectives:

1. Investigating possible boundary effects of DFN models and proposing a methodology to mitigate boundary effects on target volumetric intensity.
2. Investigating the relationship between borehole fracture intensity and volumetric fracture intensity and proposing a methodology to quantify the reliability of the volumetric fracture intensity derived from borehole fracture intensity.
3. Proposing a methodology to estimate the volumetric fracture intensity from borehole fracture intensity, avoiding increasing or decreasing artificially the volumetric fracture intensity calculated in the borehole intervals.

1.3 Thesis Organization

This thesis is organized into six chapters including the current introductory Chapter.

Chapter 2 provides a literature review of the main concepts and methods used in the development of this thesis. It includes a brief introduction to Discrete Fracture Network (DFN) modelling and different methodologies to calculate volumetric fracture intensity from the linear fracture intensity.

Chapter 3 investigates the effect of the generation box size on the target fracture intensity within a defined volume of interest, by comparing input intensity with target intensity for a series of DFN models. Then based on the results of the analyses performed, a methodology to minimize and correct the effect of boundary effects on DFN models' intensity is presented.

Chapter 4 investigates the variability in borehole fracture intensity and its relationship with the volumetric fracture intensity using DFN models. A methodology to quantify the reliability of the volumetric fracture intensity based on a given borehole fracture intensity is presented.

Chapter 5 investigates, using DFN models, the effects of the minimum bias angle and the length of the borehole intervals in the calculated volumetric fracture intensity. Based on the results of the analysis performed, a methodology to estimate the volumetric fracture intensity from borehole fracture intensity is presented. The main purpose of the methodology proposed is to capture the spatial variation in volumetric fracture intensity, while at the same time avoiding increasing or decreasing artificially the volumetric fracture intensity calculated in the borehole intervals.

Chapter 6 summarizes the research, describe its limitations, presents the key findings and conclusions, and provides recommendations for future work.

Chapter 2: Literature Review

2.1 Introduction

Chapter 2 provides a literature review of the main concepts and methods used in the development of this thesis. An introduction to Discrete Fracture Network (DFN) modelling is presented, including the key input parameters required to generate a basic DFN model. Different methodologies to obtain volumetric intensity from linear intensity are also discussed.

2.2 Discrete Fracture Network (DFN) Modelling

The Discrete Fracture Network (DFN) approach allows the characterization of discontinuities using statistical distributions to describe variables such as orientation, persistence and spatial location of discontinuities (Elmo et al., 2008). DFN modelling has become increasingly popular in recent years amongst geotechnical practitioners and engineers, including the generation of synthetic rock mass properties (Elmo and Stead, 2010), geomechanical simulation of open pits (Rogers et al., 2009; Rogers et al., 2016), quantification of rock mass pre-conditioning (Brzovic et al., 2015), estimation of rock bridge percentage for stability analysis (Dershowitz et al., 2017) and rock mass fragmentation and calculation of fragmentation distribution at cave mine scale (Rogers et al., 2015).

The main primary characteristic (Dershowit, 1984) of fracture orientation, fracture intensity and fracture size, required to generate a simple DFN model are described in the following sub-sections.

2.2.1 Fracture Orientation

It is possible to generate DFN models by applying separate statistical orientation distribution for each fracture set. This method is known as the disaggregate approach (Elmo, 2014) because

independent DFN models are generated for each set. Then, it is possible to obtain the overall representation of the fracture orientation by combining the set generated individually. Alternatively, the data can be analyzed using a bootstrap approach, in which a pseudo-replicated sample of fracture orientations is generated by multiple random sampling with replacement from an original sample. This is very useful when the original sample data is characterized by a highly disperse scatter, and when the data does not follow any clear statistical distribution.

2.2.2 Fracture Size

For DFN modelling applications, fracture size is typically described in terms of fracture radius, and therefore it becomes important to understand the difference between fracture trace length (mapped information) and fracture radius (simulated data). The first corresponds to the observed length of the trace that a fracture makes with a surface, while the former corresponds to the radius of a circle of equivalent area to a polygonal fracture (Figure 2.1).

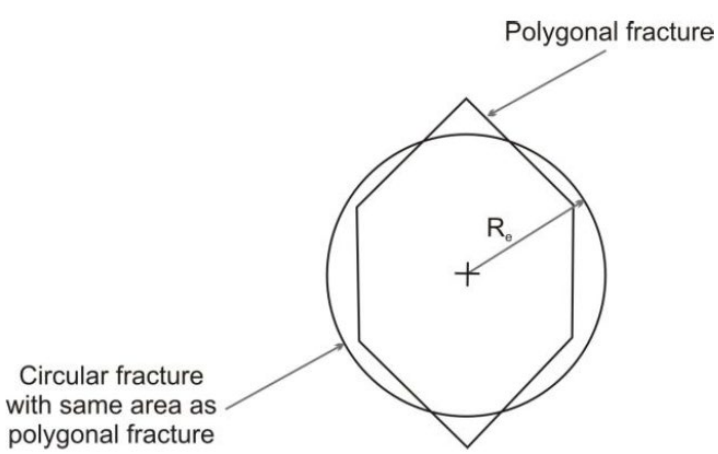

Figure 2.1: Circle of Equivalent Area for a Polygonal Fracture with n Sides and n > 3 (Elmo, 2014).

Although with the current technologies is impossible to measure fracture radius directly, fracture length can be obtained by mapping rock exposures. Then, using analytical methods (Mauldon, 1998; Zhang and Einstein, 1998 and Zhang and Einstein, 2000), the distribution of fracture radius can be derived from the distribution of trace length.

2.2.3 Fracture Intensity

Fracture intensity can have different interpretations. To avoid ambiguity and improve consistency, intensity measurements are classified based upon the dimension of the measurement region and the dimension of the fracture (Dershowitz, 1992), using an intensity notation based on the designation P_{ij}, in which the subscripts (i) represent the dimension of the feature and the subscript (j) correspond to the dimension of the sampling region (Figure 2.2). For example, a borehole intensity of fractures per metre is expressed as P_{10}, while the volumetric intensity of fracture area per sampling volume is expressed as P_{32}.

Dimension of Sample	Dimension of Measurement Region: 0D (count)	1D (length)	2D (area)	3D (volume)	
1D (wellbore, scan line, etc.)	P_{10} No of fractures per unit length of borehole	P_{11} Length of fractures per unit length			Linear Measures
2D (mapping, face, outcrop)	P_{20} No of fractures per unit area	P_{21} Length of fractures per unit area	P_{22} Area of fractures per area		Areal Measures
3D (Volume)	P_{30} No of fractures per unit volume		P_{32} Area of fractures per unit volume	P_{33} Volume of fractures per unit volume	Volumetric Measures
	Density		Intensity	Porosity	

Figure 2.2: P_{ij} Intensity Notation (based on Golder Associates (2021b)).

P_{32} is a nondirectional intrinsic measure of fracture intensity, these characteristics made P_{32} the preferred measure of fracture intensity in DFN modelling (Rogers et al., 2015). While P_{32} cannot be directly measured, it can be obtained from P_{10} or P_{21} using analytical solutions or by simulation (see Section 2.5).

2.2.4 Boundary Effects in DFN Models

DFN models may present boundary effects, and their impact can be significant when the volume used to generate the DFN model is not large enough compared to the rock mass volume under consideration. To minimize these boundary effects, Priest (1993) recommended generating fractures in a volume region much larger than the volume of interest. Samaniego and Priest (1984) indicated that a generation volume of four times the volume of interest would be sufficient to

minimize boundary effects. Note that depending on the model size this increase in the size of the generation volume may significantly increase the computation time. On the other hand, Junkin et al. (2019) indicate that it could be possible to mitigate boundary effects by including mapped traces or fracture seeds on the exterior boundaries of a DFN region. They proposed to sample the DFN model using planes to estimate P_{21} intensity in areas where the boundary effect does not exist, and then use this intensity to stochastically seed traces on the boundary of the DFN.

2.3 Fracture Intensity and Terzaghi Correction

When estimating fracture intensity from a linear or planar survey, fractures that are parallel to the survey are easily observed while oblique fractures are harder to observe. The relative difference between the orientation of the sampling borehole and the orientation of the intersecting fractures introduces a bias in favour of those fractures that are perpendicular to the borehole. This orientation bias is illustrated in Figure 2.3, in which α represents the acute angle between the scanline and the fracture. The ratio of the apparent spacing (D') to the true spacing (D) is $1/\sin\alpha$. In other words, fractures at an acute angle α are underrepresented by a factor of "$\sin\alpha$", this factor being known as the Terzaghi Weight (Terzaghi, 1965).

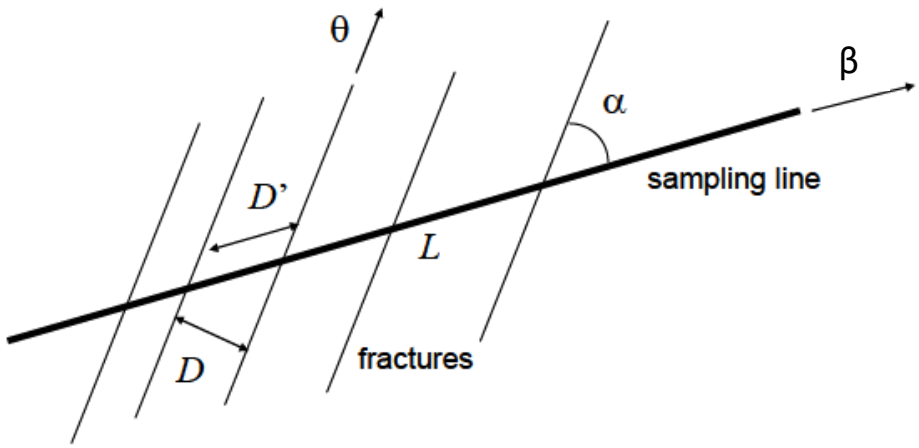

Figure 2.3: Apparent Spacing D' Associated with True Spacing D when the Fractures (direction θ) Form an Angle α With the Scanline (direction β). Adapted from (Chilès et al., 2008).

Terzaghi (1965) proposed correction for spacing (Equation 2.1), in which *d* represents the spacing, *N* the number of fractures intersected by the survey and *L* the length of the survey. Note that the Terzaghi Correction assumes a zero-thickness sampling survey.

$$d = \frac{N}{L \ \sin \alpha} \qquad \text{Equation 2.1}$$

2.3.1 Minimum Bias Angle

Since the weighting factor tends to infinity as α approaches zero (Figure 2.4), it is common to apply a maximum limit to α. Yow et al. (1987) approached this problem by considering the error associated with taking orientation measurements and linked that error (E) with the angle between the fracture and the sampling line (α), to produce an expression for the normalized maximum weighting factor error:

$$W_{Emax} = \left(\frac{\sin\alpha}{\sin(\alpha - E)}\right) x\ 100\% \qquad \text{Equation 2.2}$$

Based on Equation 2.2 and assuming an acceptable normalized maximum weighting factor error, it is possible to define the maximum weighting factor required to avoiding degrade the quality of the data. The proportional errors of the Terzaghi correction factor and the influence of the blind zone have been mathematically derived by Wang and Mauldon (2006). Priest (1993) suggests using a maximum weighting of 10, this weight corresponds to an α value of approximately 6°, while other authors recommend an α angle between 5° and 20° (Rocsience, 2022). In practice, a limit of 15° is often used, this improves the robustness of the estimator but has the inconvenience of introducing some bias by discarding valid data (Chilès et al., 2008).

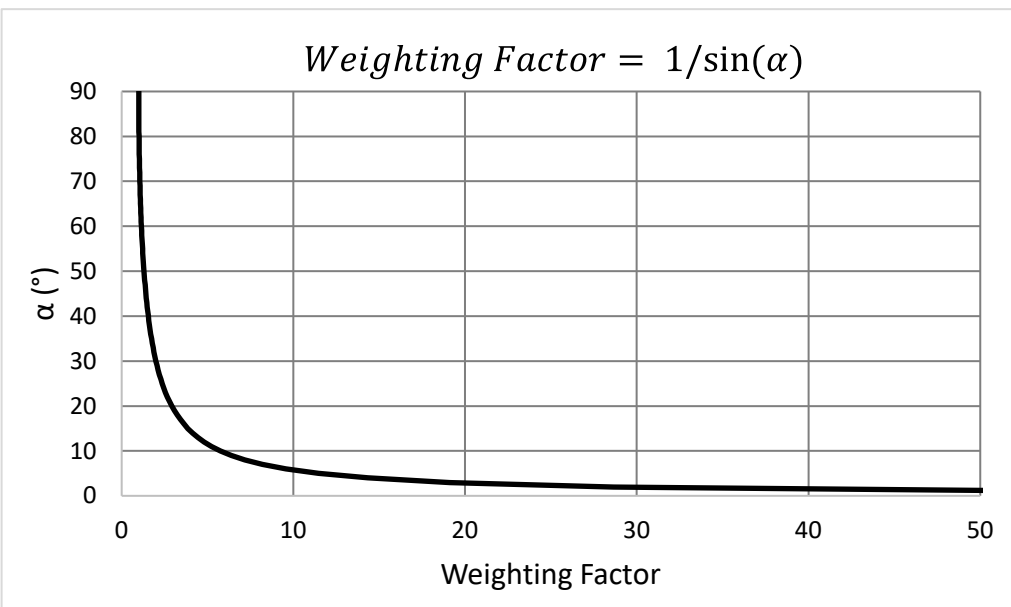

Figure 2.4: Terzaghi (1965) Weighting Factor for Different α Angles.

2.4 Mauldon Generalized Terzaghi Correction

Mauldon and Mauldon (1997) provided an improvement to the Terzaghi (1965) Correction, by calculating the probability of intersection between a fracture of known radius R and cylindrical object of radius r, thus generalizing the Terzaghi correction to the sampling by a borehole with nonzero diameter. The advantage of this method is that the correction always remains finite. The result is very useful when the fractures have a size comparable with the diameter of the survey line. However, when the fractures are much larger than the survey line the correction can be very large (Chilès et al., 2008).

2.5 Volumetric Intensity from Linear Intensity

This Section presents different methodologies to estimate volumetric intensity (P_{32}) from linear intensity (P_{10}), including the Chilès's method.

2.5.1 Chilès' Method

Chilès (Chilès et al., 2008) developed a method in which Equation 2.1 is rewritten in terms of the volumetric intensity P_{32} (Equation 2.3), and presented a generalization for the case in which fractures are sampled along a line with varying orientation or along several lines with total length L (Equation 2.4). Note that in 3D, β and ω_i are unit vectors and the factor equal to the cosine of the angle formed by the unit vectors β and ω_i corresponds to the absolute value of the inner product $< \omega_i ,\beta,>$.

$$\widehat{P_{32}} = \frac{1}{L}\sum_{i=1}^{N}\frac{1}{|\cos(\omega_i - \beta)|} \qquad \text{Equation 2.3}$$

$$\widehat{P_{32}} = \frac{1}{L}\sum_{i=1}^{N}\frac{1}{|\cos(\omega_i - \beta_i)|} \qquad \text{Equation 2.4}$$

Where L is the length of the scanline, β is its direction, β_i is the local orientation of the scanline at the location of fracture i, N is the number of fractures and ω_i the pole of fracture i.

Based on Equation 2.4, Chilès (Chilès et al., 2008) presented an estimator of the directional fracture density, in which the fracture intensity for polar direction ω is:

$$\widehat{P_{32}}(d\omega) = \frac{1}{L}\sum_{i=1}^{N}\frac{1_{\omega_i \in d\omega}}{|\cos(\omega_i - \beta_i)|} \qquad \text{Equation 2.5}$$

The advantages of this method are that it allows calculating the volumetric intensity directly from borehole intensity and that do not require knowing the fracture size or making assumptions about its distribution.

2.5.2 Chilès' Improved Terzaghi Correction

Chilès (2008) proposed an improvement to the Terzaghi correction when several surveys of length $L_1, \ldots, L_n$ and direction $\beta_1, \ldots, \beta_n$ are available. This method does not limit the minimum α angle and assumes that a fracture with a pole ω, a survey length L_s and direction β provided neither more

nor less information than a survey orthogonal to the fracture with length $L_s|\cos\omega - \beta|$. Then the fracture density for polar direction ω is:

$$\widehat{P_{32}}(d\omega) = \frac{N(d\omega)}{L(\omega)} = \frac{\sum_{i=1}^{N} 1_{\omega_i \in} d\omega}{\sum_{j=1}^{n} L_j\,|\cos(\omega_i - \beta_i)|} \qquad \text{Equation 2.6}$$

where N(dω) are fractures with poles in the solid angle $d\omega$ around ω, observed in n surveys.

In practice, when considering planar fractures, linear surveys and measurement errors, N(dω) and L(ω) are replaced by weighted averages. This approach is similar to the one proposed by Kiràly (1969) in which directional intensity is calculated relative to the orientation of three eigenvectors ($\vec{X}, \vec{Y}$ and $\vec{Z}$). The angles between the normal of the fracture plane and each of the eigenvector directions are restricted to a maximum of 89°. Note that if the intensity is calculated with respect to one plane or scanline, this is equivalent to restricting the minimum angle between the fracture and the sampling line (α) to a minimum of 1°.

The methodology proposed by Chilès provides an intensity average, based on the orientation of the survey lines. Therefore, if there is bias in the orientation of the survey lines, this average may not necessarily correctly represent the average of the area of study. On the other hand, since it is an average, this methodology does not capture local variations in intensity.

2.5.3 Intensity Conversion C13

Wang (2005) proposed a numerical approximation between P_{10} and P_{32}:

$$P_{32} = C_{13} P_{10} \qquad \text{Equation 2.7}$$

$$C_{13} = \left[\int_0^{\pi} |\cos\gamma| f_A(\gamma)\, d\gamma \right]^{-1} \qquad \text{Equation 2.8}$$

Where α is the solid angle between the survey line and the fracture normal (not to be confused with the α angle used in previous equations and that corresponds to the complement of this angle). Assuming that P_{10} sampled distributed according to a Univariate Fisher hemispherical probability distribution, the theoretical probability density function $f_A(\alpha)$ is given by:

$$f_A(\alpha) = \frac{1}{\pi} \int_{R\delta} \frac{\sin\alpha}{\sqrt{\sin^2\delta \sin^2\rho - (\cos\alpha - \cos\delta\cos\rho)^2}} \frac{k e^{k\cos\delta} \sin\delta}{e^k - e^{-k}} d\delta \qquad \text{Equation 2.9}$$

where k represents the Fisher concentration parameter; α is the solid angle between the survey line and the fracture normal; δ is the solid angle between the fracture normal and the Fisher distribution mean pole vector and ρ is the solid angle between the Fisher distribution mean pole vector and the sampling line (survey).

For α in the range $|\delta - \rho| \leq \alpha \leq \delta + \rho$, where the range of integration R_δ is given by:

$$R_\delta = [\rho - \alpha, \rho + \alpha],\ if\ \alpha \leq \rho,\ or$$
$$R_\delta = [0, 2\alpha - \rho],\ if\ \alpha > \rho$$

Equation 2.10

Note that this method assumes that the fracture population in a single set follows a Univariate Fisher hemispherical probability distribution, and the method is not suitable for use with other types of probability distributions (Golder Associates, 2021b).

No closed-form solution for Equation 2.10 exits, and the correction factor can be obtained from a table as a function of the angle between the mean pole and the survey centerline and Fisher concentration parameter. Alternatively, numerical simulation can be used to compute the full integration for a given set of fractures.

2.5.4 Volumetric Intensity Obtained from Borehole Intensity Using Simulation

The relationship between P_{32} and P_{10} can be obtained by sampling equiprobable DFN models with simulated wells with different orientations (Dershowitz, 1992), as presented in Figure 2.5. A similar process can be used to obtain P_{32} from sampled P_{21}, in which planes are used instead of simulated wells, to obtain the trace length per area. As stated by Elmo (2014) and also corroborated by Munkhchuluun (2017), P_{32} follows a linear relationship with both P_{10} and P_{21}, this linear relationship can be expressed as:

$$P_{32} = C_{31}P_{10}$$
$$P_{32} = C_{32}P_{10}$$

Equation 2.11

where the constant C_{31} and C_{32} depend on the relative orientation of the fractures to the orientation of the survey line or plane and the fracture size distribution (Elmo, 2014).

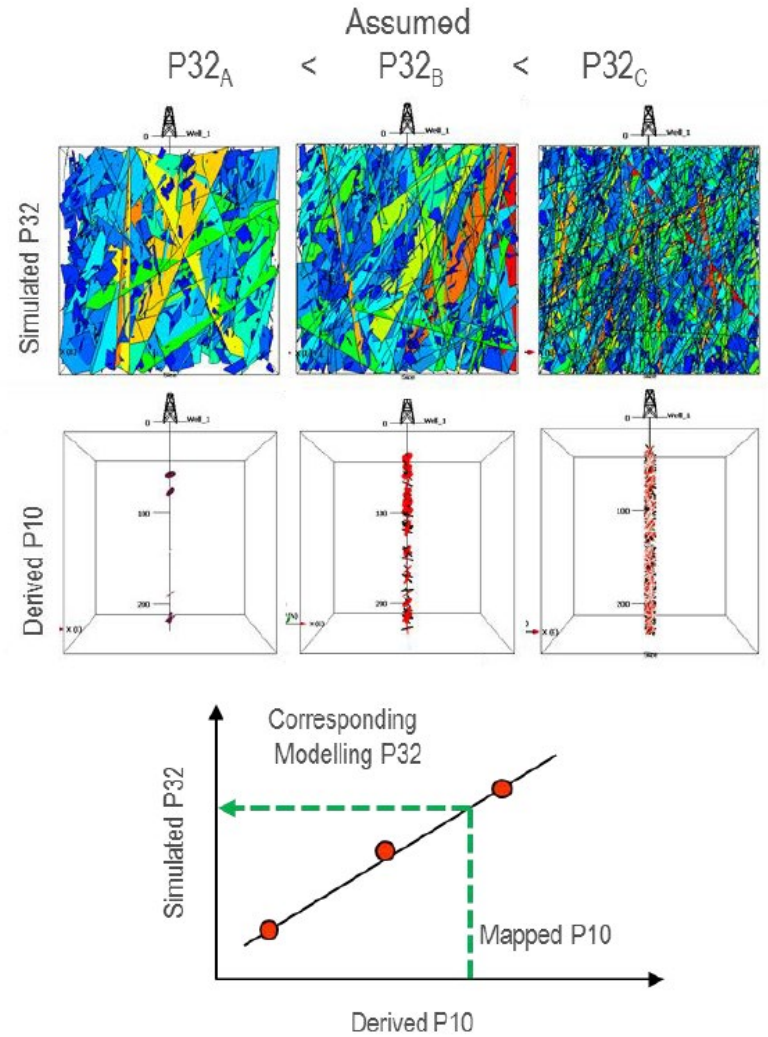

Figure 2.5: Process of Determining P_{32} by Simulation Using P_{10} (Elmo, 2014).

The main limitations of this method are that it is needed to know beforehand the fracture size distribution and orientation to generate the simulated DFN models and that the proportionality constants C_{31} and C_{32} depend on the relative orientation of the fractures to the orientation of the survey line or planes.

2.5.5 Volumetric Intensity Obtained by Combined Data Sampled on Rock Face and in Boreholes

Zhang and Einstein (2000) proposed a methodology to estimate the volumetric intensity of discontinuities by combining the data sampled on boreholes with the data sampled on exposed rock faces. This method requires estimating the discontinuity size distribution from the trace data sampled in windows.

To estimate the fracture size, Zhang and Einstein proposed a methodology to infer the fracture diameter distribution from the estimation of the true trace length distribution. The true trace length distribution can be estimated by considering circular windows and the bias associated with a circular window (Figure 2.6).

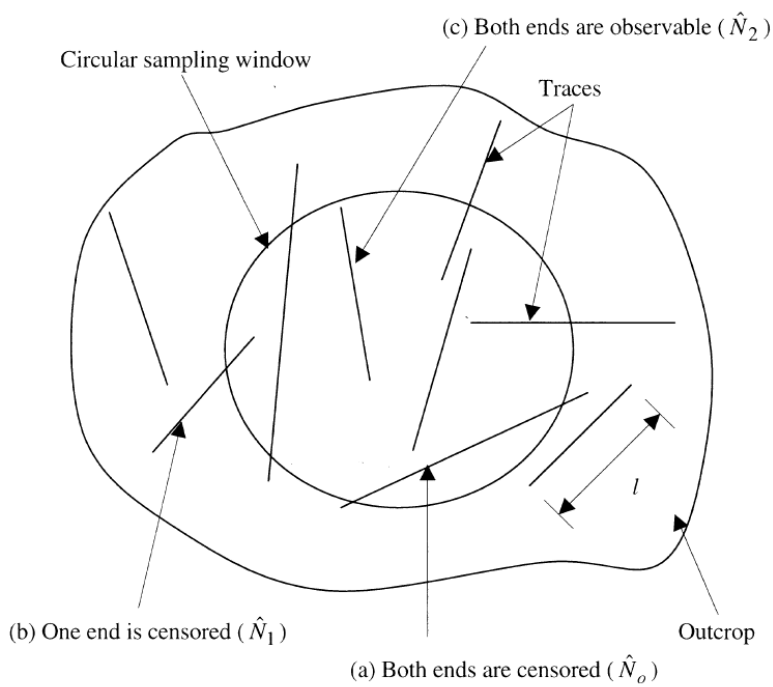

Figure 2.6: Circular Sampling Window and the Three Types of Intersection between Discontinuities and a Circular Sampling Widow, Zhang and Einstein (2000).

The stereological relationship between the true trace length distribution and the discontinuity diameter is defined as:

$$f(l) = \frac{1}{\mu_D} \int_1^{\infty} \frac{g(D)dD}{\sqrt{D^2 - l^2}} \qquad \text{Equation 2.12}$$

where D is the diameter of the discontinuities; l is the trace length of discontinuities on a planar exposure of infinite size; $g(D)$ is the probability density function of the diameter of discontinuities; $f(l)$ is the probability density function of true trace lengths and μ_D is the mean diameter of discontinuities.

Zhang and Einstein (2000) assume that $f(l)$ present the same distribution form as the probability density function of the measured trace lengths on a finite exposure $g(l)$, then by calculating its mean (μ_1) and standard deviation (σ_1) it is possible to completely determine $f(l)$.

The corrected mean μ_1 of $f(l)$ can be obtained from the observed trace length in a finite circular window (Figure 2.6) as:

$$\mu_1 \approx \hat{\mu} = \frac{\pi(\widehat{N} + \widehat{N_0} - \widehat{N_2})}{2(\widehat{N} - \widehat{N_0} + \widehat{N_2})}\, c \qquad \text{Equation 2.13}$$

where $\widehat{N}$ is the total number of traces intersecting the sampling window; N_0 is the total number of traces with both ends censored; $N_2$is the total number of traces with both ends observable; $\hat{\mu}$ is the predicted mean trace length from $\widehat{N}, N_0$ and N_2 and c is the radius of the sampling window.

Note that in Equation 2.14 when $\widehat{N} = \widehat{N_0}$, then $\hat{\mu} \to \infty$, and when $\widehat{N} = \widehat{N_2}$, then $\hat{\mu} \to 0$. These two special cases can be addressed by changing the sampling widow location and/or increasing the window radius.

Assuming that $f(l)$ and $\mathrm{g}(l)$ present the same coefficient of variation (COV), the standard deviation (σ_1) of $f(l)$ can be obtained as:

$$\sigma_1 = \mu_1 \, (\mathrm{COV}_l)_m \qquad \text{Equation 2.15}$$

were $(\mathrm{COV}_l)_m$ is the coefficient of variation of the measured trace lengths.

Once $f(l)$ is completely determined, the probability density function of the diameter of discontinuities $g(D)$ can be obtained assuming its distribution form. Zhang and Einstein (2000) provide equations describing the calculation of the Lognormal, Negative Exponential, and Gamma fit curves, based on the values of $u_1$and σ_1 (Table 2.1). Zhang and Einstein also provide expressions to check the quality of the distribution form assumed (Table 2.2), based on the mean (μ_D) and standard deviation (σ) of $g(D)$and the first ($\mathrm{E}(l)$) and third ($E(l^3)$) moments of the true trace length distribution $f(l)$.

Table 2.1: Expressions for Determining mean (μ_D) and standard deviation (σ_D) of $g(D)$ from $\mu_1$and σ_D, Zhang and Einstein (2000).

Distribution form of $g(D)$	Mean μ_D	$(\sigma_D)^2$
Lognormal	$\frac{128(\mu_1)^3}{3\pi^3[(\mu_1)^2+(\sigma_1)^2]}$	$\frac{1536\pi[(\mu_1)^2+(\sigma_1)^2](\mu_1)^4-182^2(\mu_1)^6}{9\pi^6[(\mu_1)^2+(\sigma_1)^2]^2}$
Negative Exponential	$\frac{2\mu_1}{\pi}$	$\left[\frac{2\mu_1}{\pi}\right]^2$
Gamma	$\frac{64(\mu_1)^2-3\pi^2[(\mu_1)^2+(\sigma_1)^2]}{8\pi^3\mu_1}$	$\frac{\{64(\mu_1)^2-3\pi^2[(\mu_1)^2+(\sigma_1)^2]\}\{3\pi^2[(\mu_1)^2+(\sigma_1)^2]-32(\mu_1)^2\}}{64\pi^2(\mu_1)^2}$

Table 2.2: Expressions for Checking the Quality of the Distribution Form Assumed, Zhang and Einstein (2000).

Distribution form of $g(D)$	Expression	$Note$
Lognormal	$\frac{[(\mu_D)^2+(\sigma_D)^2]^5}{(\mu_D)^8}=\frac{4E(l^3)}{3E(l)}$	The best distribution form of $g(D)$ is the form which the left and right sides of the expression are closest to each other.
Negative Exponential	$12(\mu_D)^2=\frac{4E(l^3)}{3E(l)}$	
Gamma	$\frac{[(\mu_D)^2+2(\sigma_D)^2][(\mu_D)^2+3(\sigma_D)^2]}{(\mu_D)^2}=\frac{4E(l^3)}{3E(l)}$	

The total number of fractures in an objective volume can be estimated using the discontinuity diameter distribution $g(D)$ and the probability that a discontinuity with its centroid in the objective volume will intersect a borehole. Then the volumetric fracture intensity can be calculated as:

$$P_{32} = \frac{1}{V} \sum_{k=1}^{m^{(V)}} S^{(k)} \qquad \text{Equation 2.16}$$

where V is the volume considered; $S^{(k)}$is the entire area of the kth discontinuity and $m^{(V)}$ is the number of discontinuities in the volume V.

The problem with this methodology is that it requires exposed rock faces, something that is not always available, particularly in the initial stages of a project. Also, even if surface data is available this may not be representative of the underground conditions.

2.6 Chapter 2 Summary

In this chapter, an introduction to DFN modelling was presented, including the main properties of orientation, size and intensity needed to generate a basic DFN model. Fracture intensity is one of the key properties in DFN modelling, the nondirectional characteristics of P_{32}, made it the preferred measure of fracture when generating DFN models. Since P_{32} cannot be measured directly, different methodologies to calculate P_{32} from P_{10} were presented. Of the methodologies presented, Chilès' (2008) methodology, consistent with the Terzaghi Weight (1965), provides the best alternative when only borehole data is available, because it allows the direct calculation of volumetric intensity from borehole data, without the need for knowing the distributions of sizes of the fractures. Note that even though the size is not needed to define the intensity when using Chilès'

methodology, the size and orientation of fractures are required to build a DFN model. In Chapter 4 the relationship between P_{32} and P_{10} will be investigated using simulation for different fracture sizes, while in Chapter 5 the methodology proposed by Chilès (2008) will be assessed using different minimum bias angles.

Chapter 3: DFN model boundary effects

3.1 Introduction

Boundary effects are often disregarded by the engineering community when generating DFN models. This Chapter is dedicated to the study of the boundary effects that may influence the intensity of DFN models. A series of DFN models were generated using Fracman Software Version 8.1 (Golder Associates, 2021a), and a new methodology is then proposed to minimize and correct the effect of boundary effects on DFN models' intensity.

3.2 DFN Modeling to Investigate Possible Boundary Effects on Intensity

In order to determine and quantify the impact of boundary effects on volumetric fracture intensity (P_{32}), a set of DFN models were generated within a box of 150 m per side. P_{32} values were then calculated using progressively smaller boxes (Figure 3.1). The input P_{32} values were compared with the P_{32} obtained for the different volumes. The goal of this modelling exercise was to quantify the effect of the generation box on the target intensity of the models.

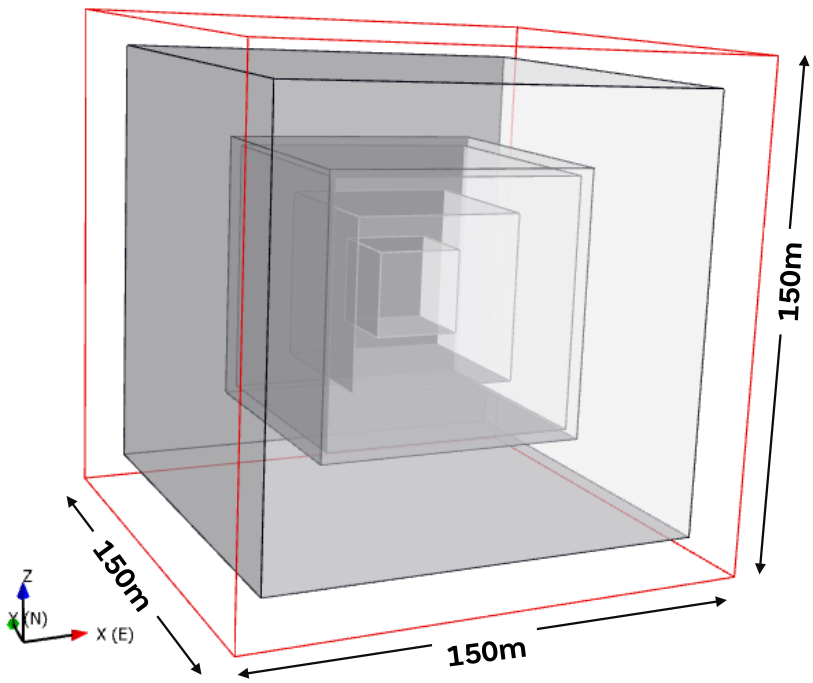

Figure 3.1: Generation Box (in Colour Red) and Sampling Boxes Used to Calculate P_{32} (in Colour Grey). Note that for Illustrative Purposes Only Some of the Sampling Boxes are Shown.

Fracture locations were generated using both points and surface centres. For points, the generation point is the centre of the fracture, while in surface point, the generation point of the fracture is a random point within the fracture. According to the Fracman Manual (Golder Associates, 2021b), this option can reduce boundary effects when generating P_{32} values. Table 3.1 summarizes the properties used in the initial models.

Table 3.1: Input Parameter Used in the Models to Investigate Boundary Effects.

Property	Note
Orientation	Bootstrapped using a concentration parameter of 80 and the orientations presented on Figure 3.2
Spatial model	Enhanced Baecher with generation locations at fracture centre and surface point
Intensity P_{32} (m^{-1}) value	2
Size: Lognormal Distribution	Radius Mean (X_{mean}): 2-5-10-15-20-25 (m) and Standard Deviation (SD) of 40 % of the mean radius size
Fracture Shape	Hexagon with a constant aspect ratio of 1
Number of equiprobable realizations	100 per scenario (1,200 realizations)

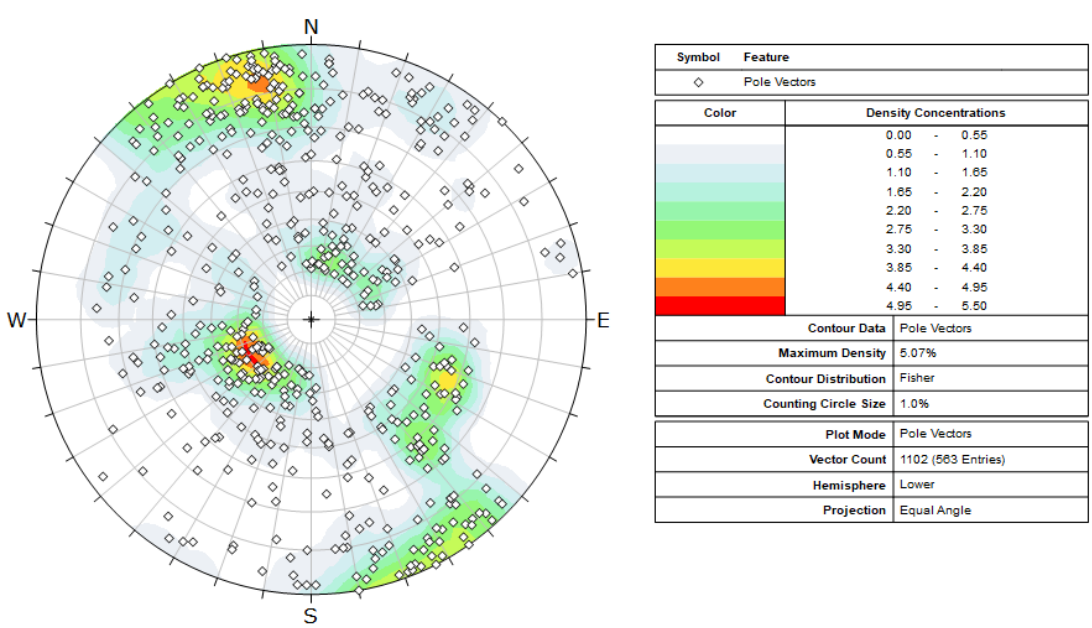

Figure 3.2: Stereonet with Orientation Used for Bootstrapping, 563 Poles Including Terzaghi Weight.

3.3 Results

Figure 3.3 summarizes the results for a mean fracture radius size of 20 m and a P_{32} input of 2 m^{-1}. The results show a difference up to approximately 30% between the input intensity and the target intensity, thus demonstrating that the intensity can be highly affected by boundary effects.

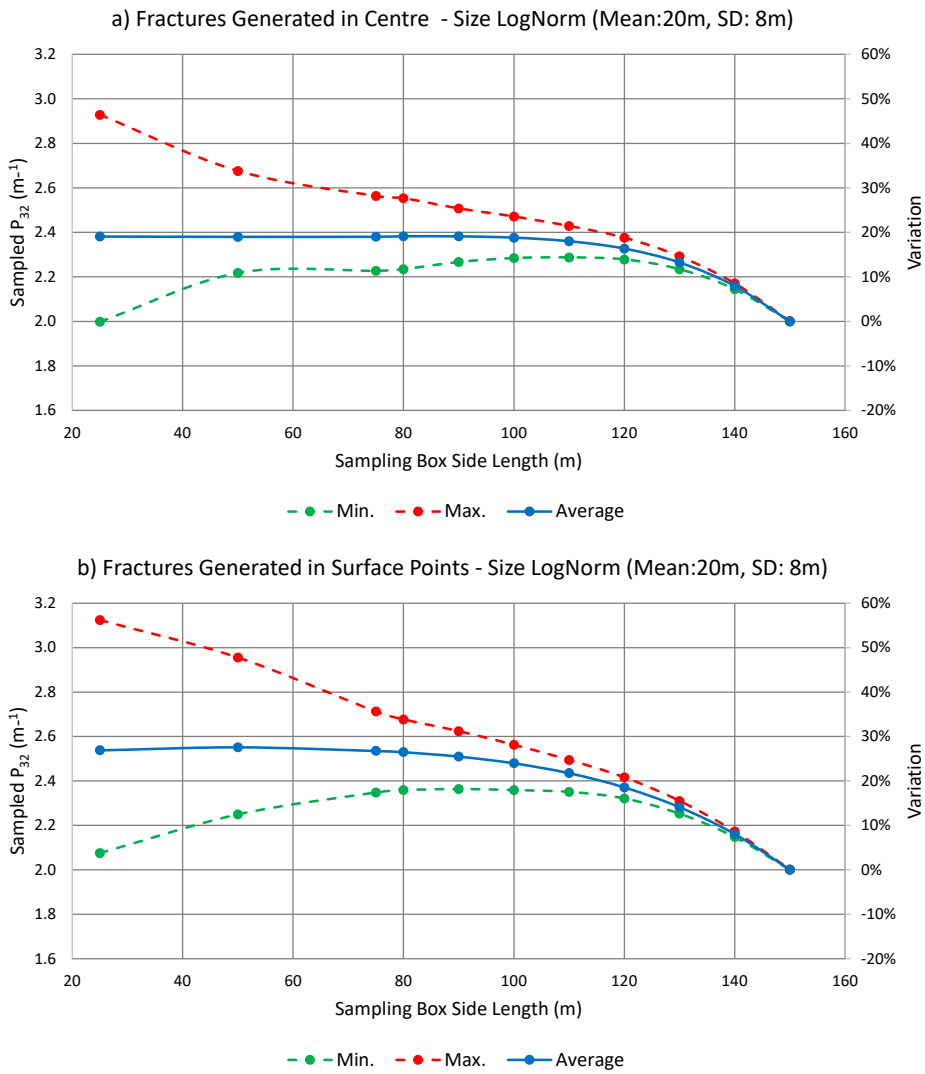

Figure 3.3: Boundary Effect and Effect of the Sampling Box in Sampled P_{32}. Figure 3.3a: Using Fractures Generated in Centres. Figure 3.3b: Using Fractures Generated in Surface Points.

As shown in Figure 3.3, P_{32} sampled at a scale corresponding to the generation box yields the input P_{32}, but as the volume of the sampling region is progressively reduced (assuming the coordinates of the center of every generation volumes remain the same), the average P_{32} value increases showing an asymptotic behaviour. Contrary to what may be expected, the models with fractures generated using its centre as reference present a better agreement with the input P_{32}, and the average curve stabilizes faster than the one for the models in which fractures are generated using the surface points option.

The variability increases as the sampling box size decrease, meaning that the ratio between sampling box size and fracture size influences the variability. For the case in which fractures are generated at the centre point, there is a marker change in the slope of the curves for the maximum and minimum values when the edge length of the generation volume is twice the fracture radius.

The difference between input P_{32} and sampled P_{32} can be explained if one considers that the Baecher model (Baecher et al., 1978) - used as a standard spatial model by many engineers and practitioners – assumes that fractures are located uniformly in space, meaning that the fractures with generation points located outside the generation box and at a distance from the boundary smaller than a fracture diameter are not generated. In a hypothetical infinite generation space, those fractures would extend back into the original boundary box, but in a constrained model this results in a lower intensity near the boundary, this boundary effect was already described by Priest (1993), who recommended to analyzing a volume of interest that is smaller than, and at the centre of, the generation volume. Note that the size of the generation box will depend on the fracture size distribution. Samaniego and Priest (1984) indicated that using a sampling area located at the central quarter of the generation volume minimizes the boundary effects. Depending on the model size

this may significantly increase the computation time, and since the boundary effect is related to the fracture size, this may not reduce the boundary effect completely.

The asymptotic behaviour observed in Figure 3.3, indicates that it is possible to define a correction factor for the input P_{32}. This factor will be dependent on the size of the volume of interest, the size of the generation box, the fracture size distribution, and the fracture orientation. As an example, let us consider a model with a mean fracture size of 20 m and fractures generated at the centre point. For this model, DFNs were generated considering a target intensity P_{32} of 2 m^{-1}, a volume of interest of 100 m per side and an input intensity, applied at the generation box of 150 m per side, calculated as 84% of the target intensity within the volume of interest. This reduction of 84% corresponds to the factor in which the average curve of P_{32} stabilizes ($\frac{2.00}{2.38}$ = 84% of average sampled P_{32} presented on Figure 3.3a). The results of this exercise are presented in Figure 3.4.

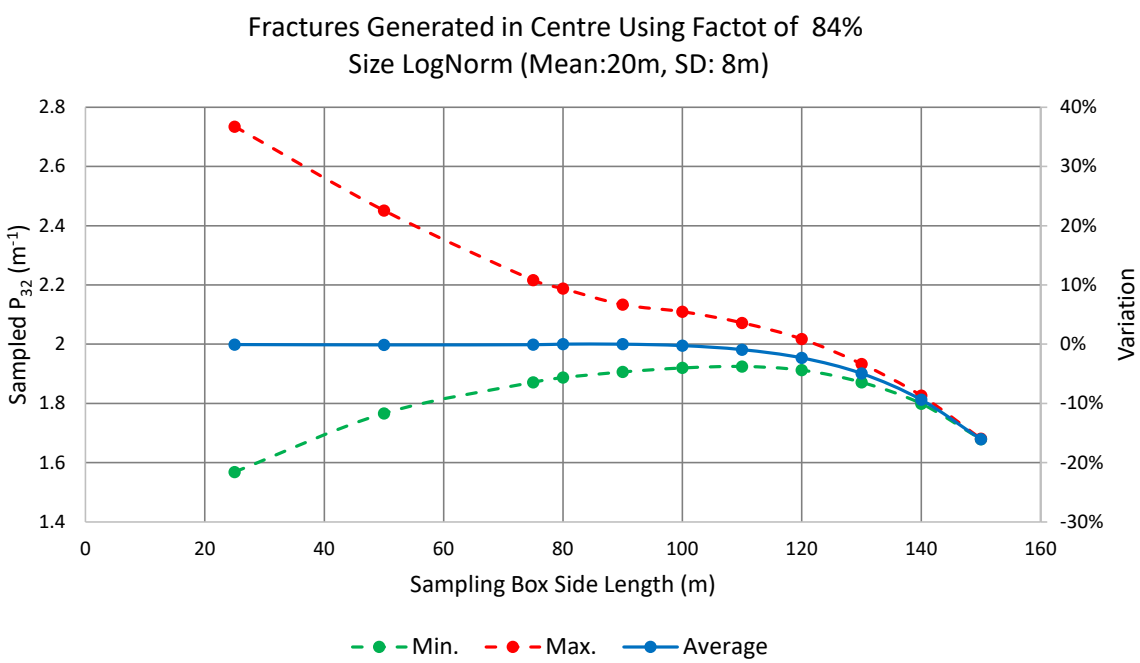

Figure 3.4: Effect of Correction Factor in Target intensity.

It can be observed in Figure 3.4 that using this methodology it is possible to obtain the target P_{32} of 2 m^{-1} on the volume of interest and that the curve stabilizes approximately at a distance of 50 m from the border of the generation box. This distance is slightly lower than 3 times the mean fracture radius (60 m). Based on these results, models were generated for a range of fracture sizes (Table 3.1), using a generation box size of 100 m plus 3 times the mean fracture radius, this assuming that the volume of interest corresponds to a box of 100 m per side. The results of this exercise are presented in Figure 3.5 and show that for the assumed fracture orientation and size, it is possible to avoid the boundary effects when using a generation box size of 100 m plus 3 times the mean fracture size.

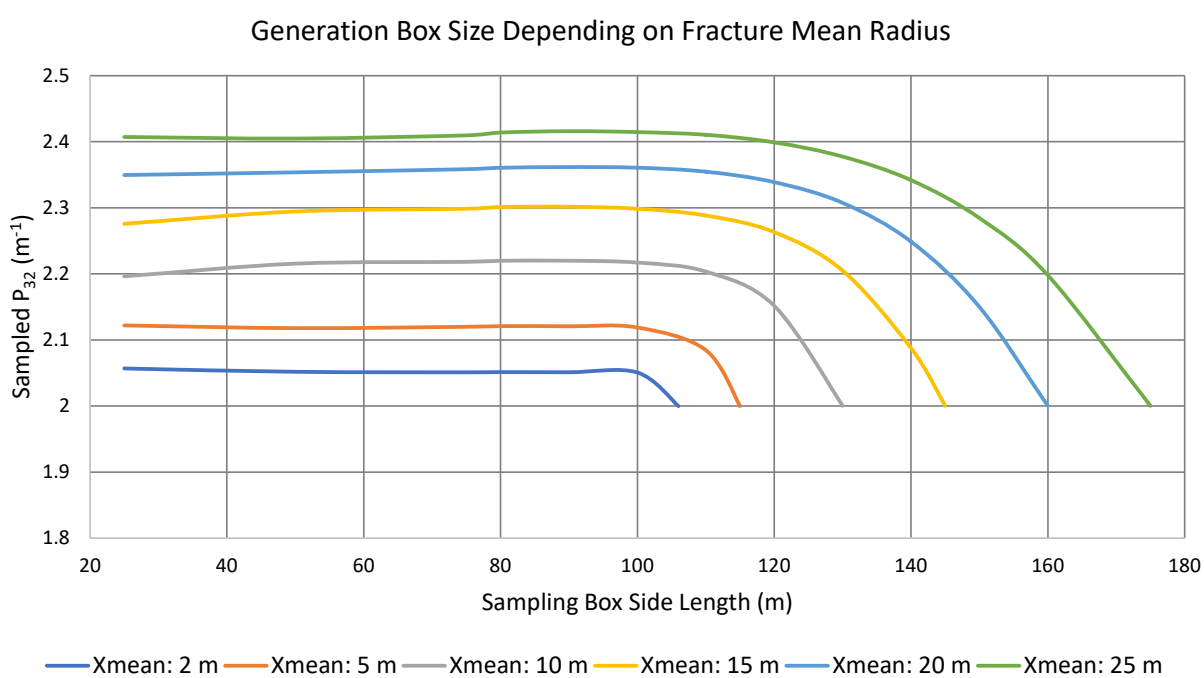

Figure 3.5: Effect of Box Size on Intensity, Using Generation Box Sizes Depending on Fracture Mean Radius.

To investigate the number of realizations required to obtain a meaningful sampled average P_{32} in the volume of interest, the cumulative average of the sampled P_{32} was plotted against the number of realizations (Figure 3.6). This provides a graphical representation that allows determining whether or not the number of realizations are converging to a constant sampled P_{32}.

As shown in Figure 3.6, the number of realizations required will depend on the size of the fractures. When fractures are small the plot converges quickly meaning that just a small number of realizations are needed to obtain a meaningful average P_{32}. Conversely, when the fracture size increases a greater number of realizations are required for the results to converge. The analysis shows that for a mean fracture radius of 25 m, approximately 30 to 50 realizations are required, while for a mean fracture radius of 2 m, as few as 10 realizations may be sufficient to obtain a representative mean P_{32}. Note that if the plots do not converge, then the number of realizations should be increased.

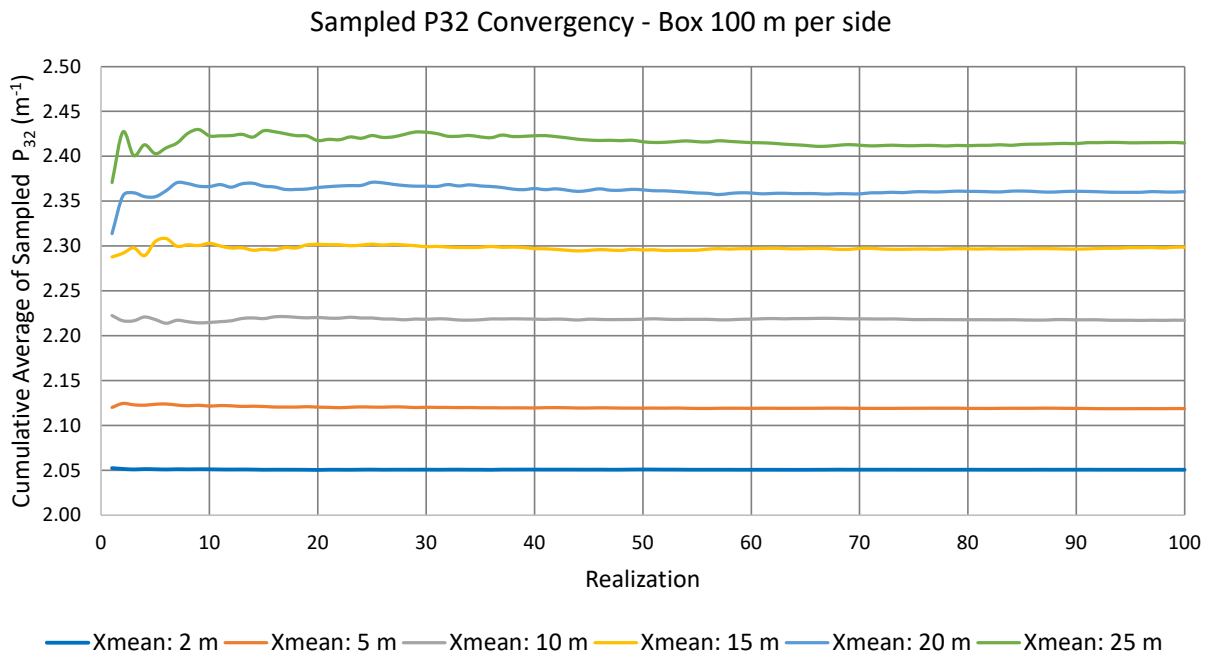

Figure 3.6: Cumulative Average of Sampled P_{32} for a Box of 100 m per Side (Volume of Interest).

3.4 Effect of Input Intensity on Target Intensity

The effect of the input intensity was investigated by generating models with different intensities and comparing the variation in percentage between the input P_{32} and the P_{32} sampled in region volumes of different sizes. For this exercise, fractures were generated in a generation volume with side length of 125 m, using the properties presented in Table 3.1. Table 3.2 shows the results of this exercise for a mean fracture radius of 25 m.

Table 3.2: Percentage Variation Between Input P_{32} and Sampled P_{32} for Fractures with a Mean Radius of 25 m.

Length of Box Side (m)	Input P_{32}				
	1 (m^{-1})	2 (m^{-1})	3 (m^{-1})	4 (m^{-1})	5 (m^{-1})
25	27.6%	24.2%	23.9%	23.9%	23.7%
50	25.0%	24.0%	23.9%	24.0%	24.1%
75	23.8%	23.4%	23.3%	23.3%	23.4%
100	18.4%	18.3%	18.3%	18.3%	18.4%
125	0.0%	0.0%	0.0%	0.0%	0.0%

It can be observed in Table 3.2 that for a defined box size, the variation in percentage, with respect to the input intensity, is relatively constant. This suggests that if the other properties are maintained constant, the correction factor is independent of the fracture intensity; therefore, the same correction factor can be applied to models with different intensity values. This will be useful in Chapter 4, in which the relationship between linear intensity and volumetric intensity will be investigated for a range of intensities.

3.5 Methodology Proposed to Avoid Boundary Effect on Intensity

Based on the results presented in this Chapter, a methodology is proposed to mitigate the impact of boundary effects on intensity when using DFN models generated in regions with different sizes.

1. Define a Volume of Interest, this volume corresponds to the volume in which we want to define the target P_{32}.

2. Generate fractures in a region bigger than the volume of interest. The size of the generation volume depends on the mean fracture size and its standard deviation. A sensitivity analysis could be performed to estimate the size of the generation volume.
3. Run an adequate number of realizations with an initial P_{32} close to the target P_{32}. The number of realizations to perform will depend on the fracture size distribution. Cumulative average plots can be used to estimate the appropriate number of realizations. If the plots do not converge, then the number of realizations should be increased. Conversely, if the curves converge quickly to the average sampled P_{32}, then it is possible to decrease the number of realizations, this will decrease the total computation time, obtaining similar results.
4. Calculate P_{32} in the volume of interest and other smaller volumes to check that the curve of average sampled P_{32} has stabilized for the volume of interest. If the curve has not stabilized, it is necessary to increase the size of the generation region (go back to step 2).
5. If for the volume of interest, the curve is in the asymptotic stretch, calculate the average P_{32} in the volume of interest and the ratio between input P_{32} and the average P_{32}.
6. Rerun the model using the initial P_{32} multiplied by the correction factor.
7. Check that the P_{32} in the volume of interest corresponds to the target P_{32} within an acceptable margin of error. If the error is greater than the acceptable error, go back to step 6. Note that to avoid going back to Step 6, it is possible to generate several DFN models and keep only the ones that comply with the acceptable margin of error. For the purpose of this Thesis, a difference of ± 1% of the target intensity has been adopted.

Figure 3.7 presents a flowchart with the methodology proposed to avoid boundary effect on intensity.

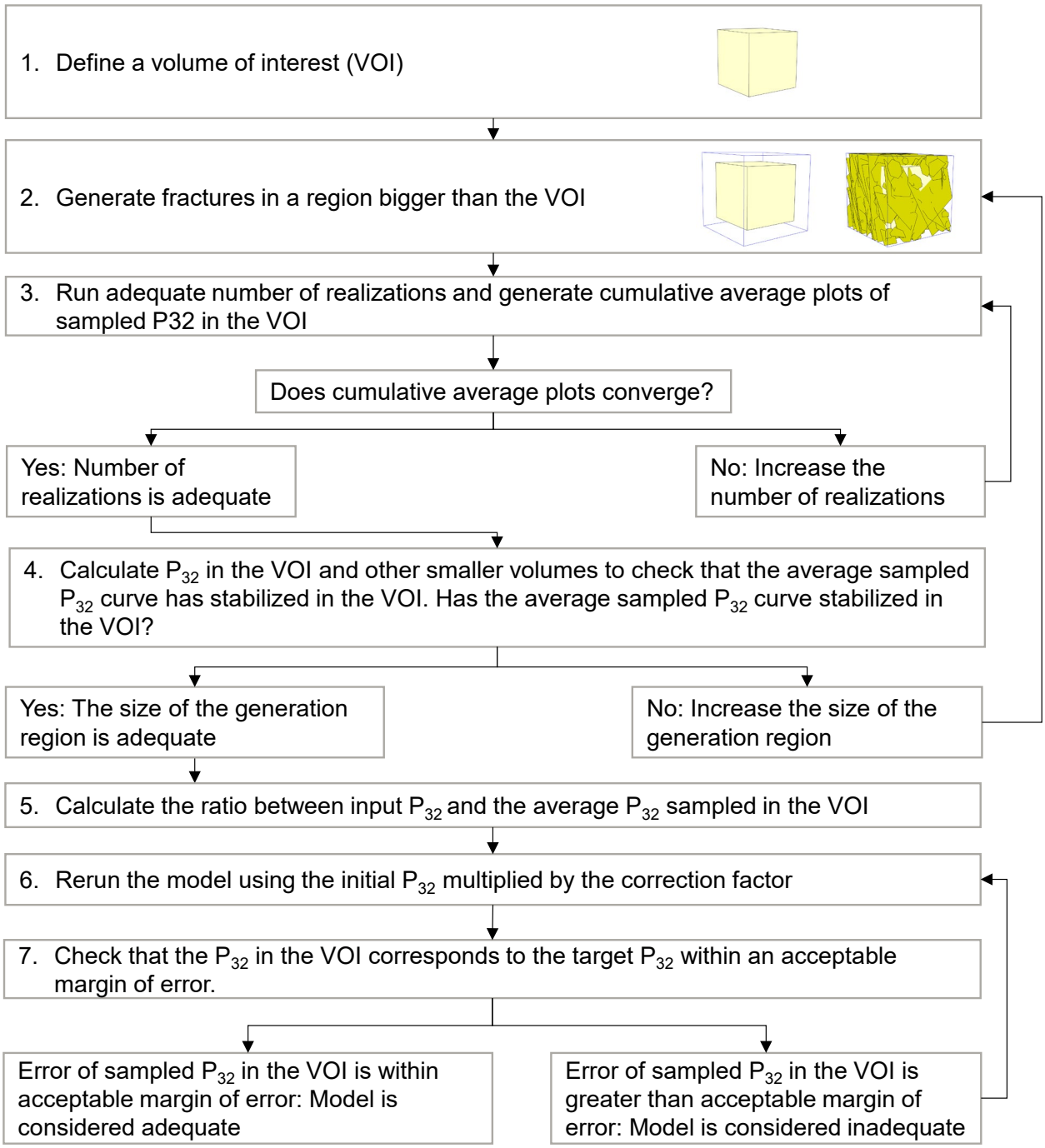

Figure 3.7: Flowchart with the Methodology Proposed to Avoid Boundary Effect on Intensity.

3.6 Chapter 3 Summary

Boundary effects are often ignored when building DFN models. In this Chapter we have discussed the impact of boundary effects in DFN models and proposed a method to address it. The proposed method considers both fracture size and the dimensions of the volume of interest. When applied, the method allows to generate models that honour the target intensity within the volume of interest.

Chapter 4: Variability and Borehole Intensity and Its Relationship with Volumetric Intensity

4.1 Introduction

The goal of the of the Chapter is to better characterise the relationship between the volumetric intensity (P_{32}) and the linear fracture intensity (P_{10}), and to quantify the reliability of the intensity parameters and its variation. As part of this study, we have considered DFN models in which we changed key input parameters, namely P_{32} and fracture size. A methodology to estimate P_{32} using simulation and its variability for a given P_{10} is then presented.

4.2 DFN Model Definition and Input Parameters

48 DFN models were generated in Fracman Software Version 8.1 (Golder Associates, 2021a) using as volume of interest a 100 m x 100 m x 100 m box region (centred in the origin) and the properties presented in Table 4.1. To avoid boundary effects, fractures were generated using the methodology proposed in Chapter 3. Fractures were generated within a region volume with a variable side length, equal to 100 m plus 3 times the mean fracture ratio. Once the DFN models were generated, the intensity P_{32} was sampled in the volume of interest and only models with a difference smaller than 1% of the target intensity were considered.

Table 4.1: Input Parameter Used in the Models to Investigate the Reliability of Borehole Derived Intensity

Property	Note
Orientation	Bootstrapped using a concentration parameter of 80 and the orientations presented on Figure 4.2
Spatial model	Enhanced Baecher with generation locations at fracture centre
Intensity P_{32} (m^{-1}) values	1 – 2 – 3 – 4 – 5 – 6 – 7 – 8
Size: Lognormal Distribution	Radius Mean (Xmean): 2-5-10-15-20-25 (m) and Standard Deviation (SD) of 40 % of the mean radius size
Fracture Shape	Hexagon with a constant aspect ratio of 1
Number of equiprobable realizations	100 realizations with sampled intensity ± 1% of target intensity per scenario (4,800 valid realizations in total)

The DFN models were sampled using 10 synthetic wells (Figure 4.1), and the orientations of the wells (boreholes) were defined trying to cover the whole stereonet area. Table 4.2 presents the coordinates and orientations of the wells used, while Figure 4.2 shows the fracture orientations used as input and blue lines representing the blind zones of each well. Terzaghi (1965) introduced the term blind zone of a drill hole to describe the locus of the poles of joints that are parallel to the drill hole and are less likely to be observed. Note that for illustrative purposes the blind zones of each well are presented only as a line, but all poles near that line (normally ±20° from the line) are less likely to be observed in that particular well.

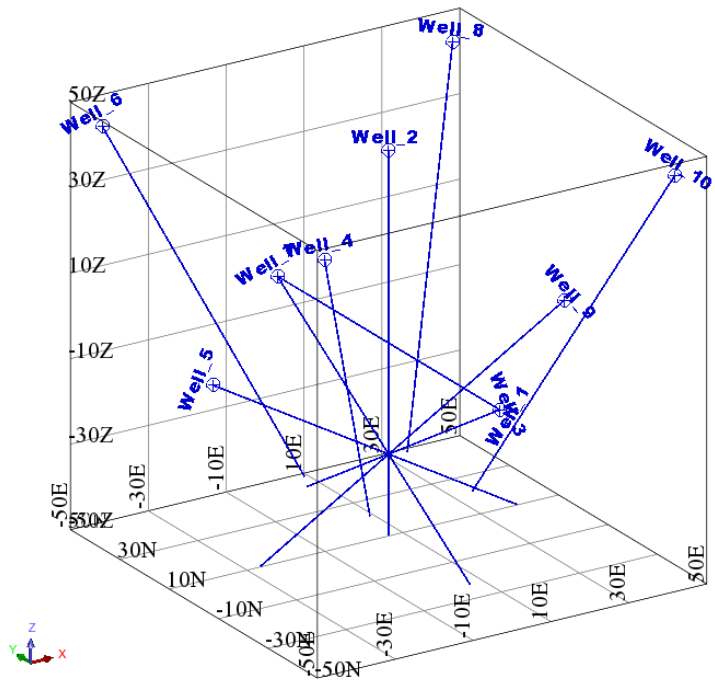

Figure 4.1: Location of Synthetic Wells, Oblique View from the Southwest.

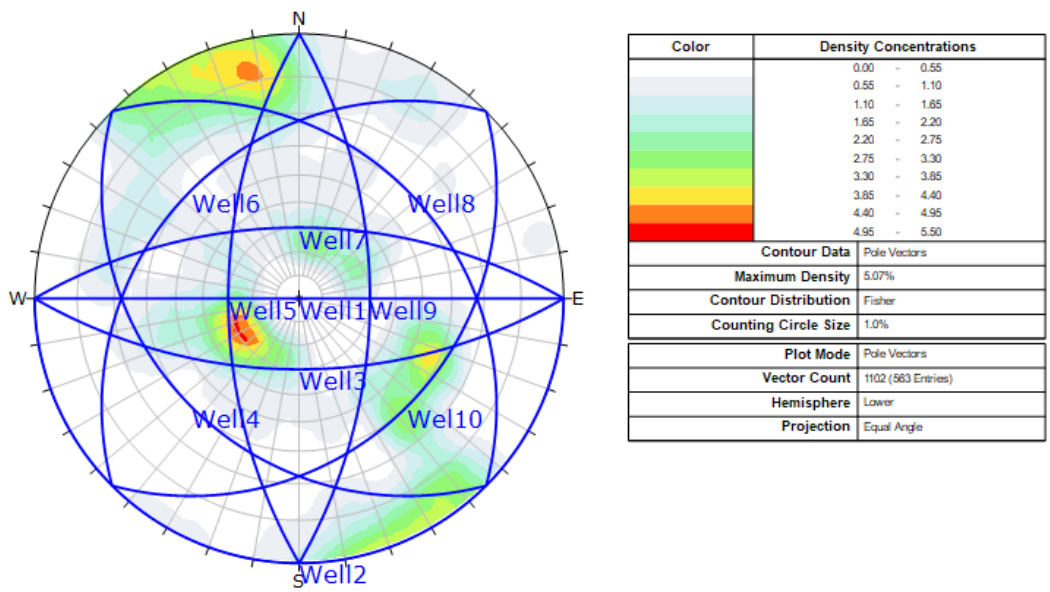

Figure 4.2: Stereonet with Orientation Used for Bootstrapping. Blind Zones of each Well are presented as blue lines.

Table 4.2: Synthetic Wells Coordinates and Orientations.

Well	East (m)	Nort (m)	Elevation (m)	Length (m)	Trend (°)	Plunge (°)
Well 1	0	-45	0	90	000	0
Well 2	0	0	45	90	000	90
Well 3	0	-45	0	90	000	30
Well 4	-45	-45	45	90	045	60
Well 5	-45	0	0	90	090	30
Well 6	-45	45	45	90	135	60
Well 7	0	45	0	90	180	30
Well 8	45	45	45	90	225	60
Well 9	45	0	0	90	270	30
Well 10	0	-45	0	90	315	0

4.3 Model Results

When sampling the DFN models with the synthetic wells, a linear relationship between input P_{32} and sampled P_{10} was observed, this linear relationship was already demonstrated using DFN modelling by Dershowitz (1992) and Elmo (2014). When the models are generated using the methodology proposed in Chapter 3 to mitigate the boundary effects, the relationship between P_{32} and P_{10} is independent of the fracture size used, note that the fracture size is a parameter that is not possible to quantify directly in boreholes. The most important consequence of this is that P_{32} can be estimated directly from borehole intensity. Figure 4.3 shows the linear relationship observed between input P_{32} and P_{10} sampled for different input intensities and fracture sizes. As expected, greater sampled P_{10} dispersion is observed for greater values of input P_{32}.

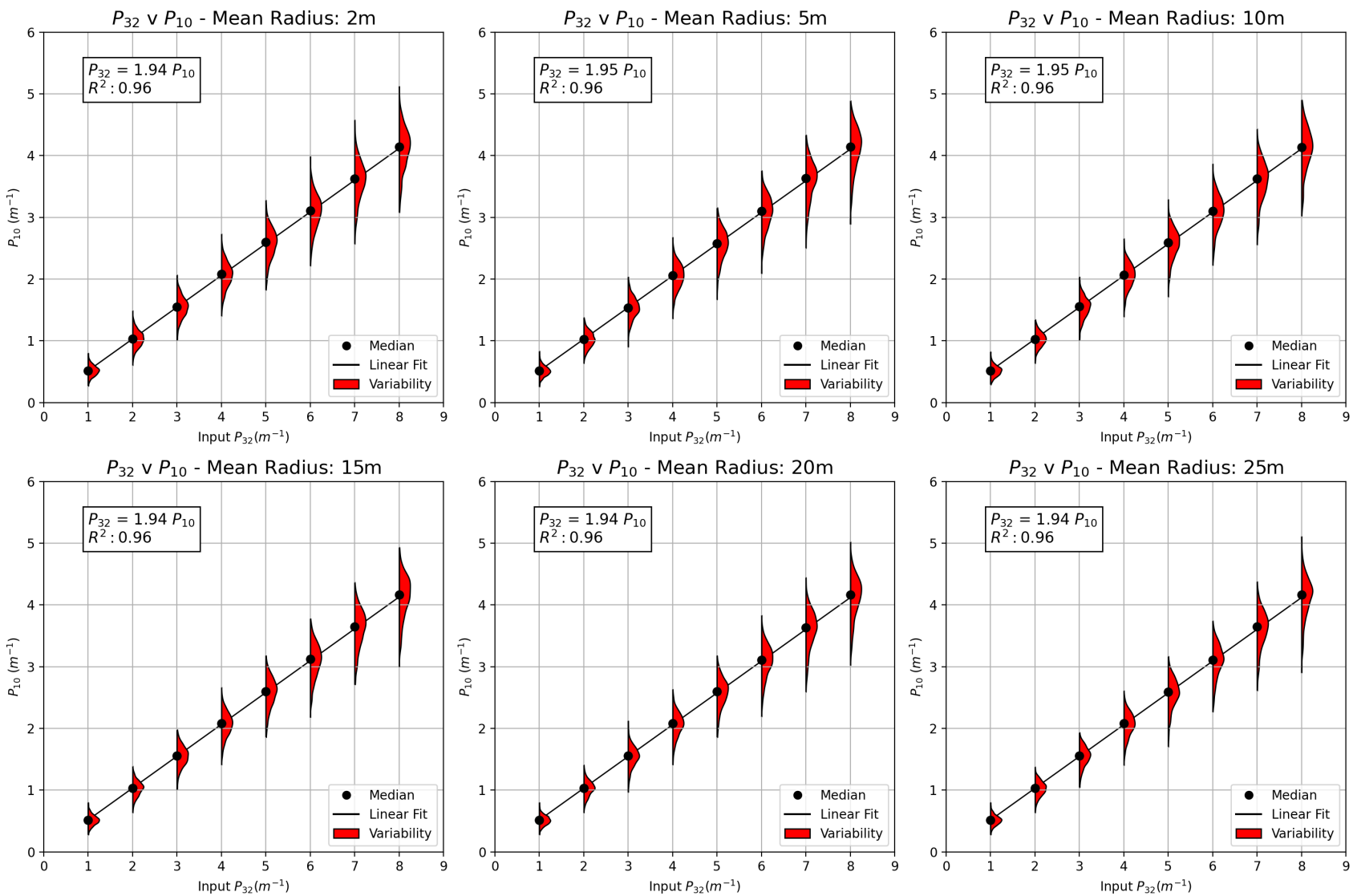

Figure 4.3: Sampled P_{10} in Wells for a Given Input P_{32}.

Table 4.3 presents the calculated ratio between input P_{32} and sampled P_{10}. As expected, the wells that present more fractures near their blind zone, present the greatest ratios. While the wells that present few fractures near their blind zone present the lower ratios. In this case, the well that presents the higher ratio corresponds to Well 5, whose blind zone intersects two pole concentrations (Figure 4.2). For this well, P_{32} is on average 2.3 times the average P_{10}.

Table 4.3: Ratio Between Input P_{32} and Sampled P_{10} per Well.

Well	Number of Realizations	Minimum Ratio	Maximum Ratio	Average Ratio	SD Ratio
Well 1	4,800	1.41	3.10	1.90	0.16
Well 2	4,800	1.25	3.10	1.87	0.16
Well 3	4,800	1.38	3.33	1.96	0.17
Well 4	4,800	1.29	3.60	2.05	0.18
Well 5	4,800	1.61	3.91	2.34	0.22
Well 6	4,800	1.30	2.90	1.88	0.15
Well 7	4,800	1.22	2.90	1.83	0.14
Well 8	4,800	1.22	3.21	1.96	0.17
Well 9	4,800	1.38	3.75	2.07	0.18
Well 10	4,800	1.20	3.00	1.82	0.15

When plotting the probability density of the sampled P_{10}, it is observed that P_{10} values are normally distributed, and when considering changes in fracture intensity, the mean and standard deviations show a linear relationship. Figure 4.4 presents an example of the probability distribution obtained

for an input intensity of 2 m^{-1}, and the linear relationship obtained between the mean and standard deviation of sampled P_{10}, for a range of input P_{32} modelled.

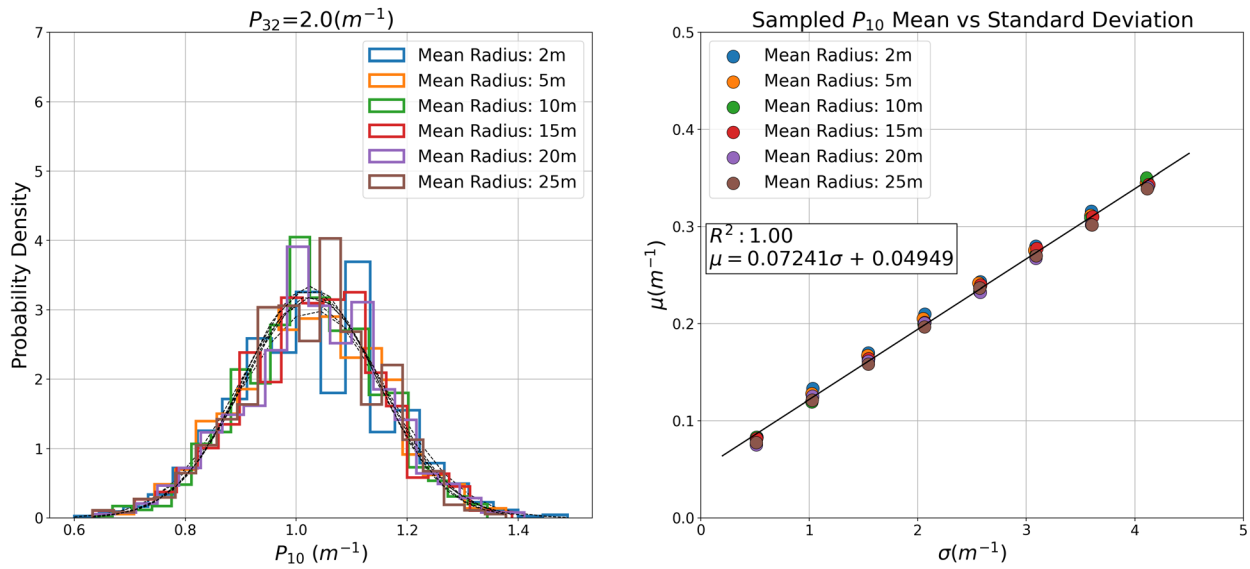

Figure 4.4: Left: Sampled P_{10} Probability Distribution for an Input P_{32} of 2 m^{-1}, Black Dashed Lines Correspond to Normal Distributions Using the Mean and SD of Each Data Set. Right: Mean (μ) and Standard Deviation (σ) of Sampled P_{10} Follow a Linear Relationship.

The results show that the mean and standard deviation of the sampled P_{10} follow a linear relationship. Therefore, for a given fracture orientation it is possible to estimate the P_{10} variability for any given P_{32} using a normal probability function. Since P_{10} and P_{32} follow a linear relationship, using probability functions and interpolation, it is then possible to estimate the variability of P_{32} for any given P_{10}.

As an example, Figure 4.5 shows the P_{32} variability obtained for a P_{10} of 2.5 m^{-1}. Note that the purpose of this exercise was to show that for a given P_{10} it is possible to obtain a range of P_{32} values with a certain degree of confidence. The limitation of this methodology is that to know the

variability of P_{32} for a given P_{10}, it is necessary first to obtain the relationship between P_{32} and P_{10} by simulation.

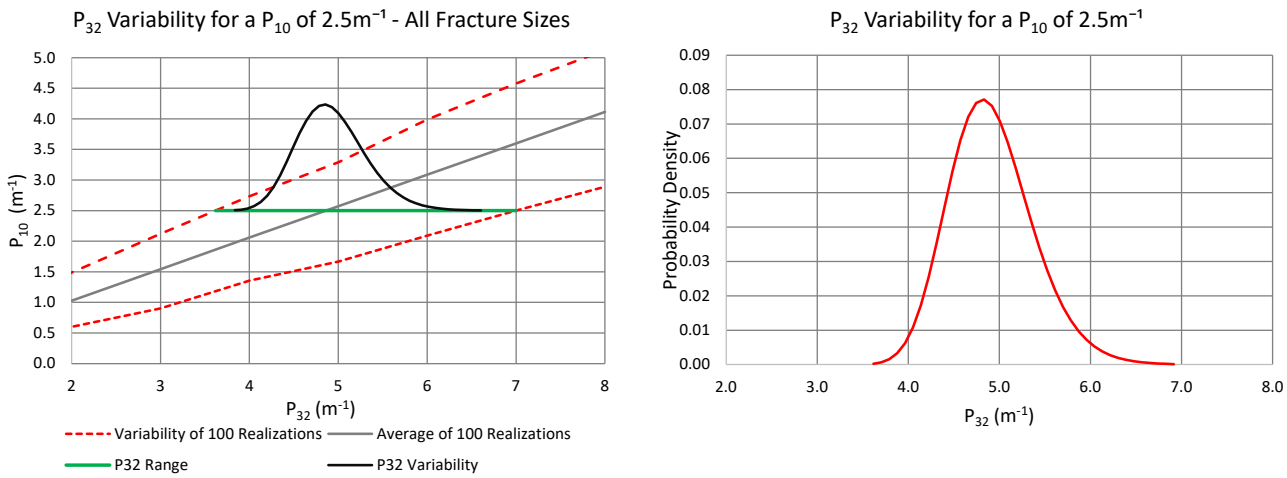

Figure 4.5: Left: Estimated P_{32} Variability for a P_{10} Value of 2.5 m^{-1}. Right: Estimated P_{32} Probability Distribution.

4.4 Recommended Methodology to Estimate Volumetric Intensity Using Simulation

If we consider that the intensity is not affected by fracture size, and that follows a linear relationship between P_{10} and P_{32}, we can estimate the volumetric intensity using DFN modelling. Another advantage of using DFN modelling is that it is possible to run several realizations and quantify the variability and distribution of the volumetric intensity for a given linear intensity. The following methodology is recommended:

1. Define a volume of interest and follow the methodology proposed in Chapter 3 to reduce boundary effects.
2. Since the relationship between P_{10} and P_{32}, is dependent of the orientation of the fracture with respect to the sampling survey (borehole), it is recommended to use the same

orientation as the actual boreholes in which the intensity was measured. Synthetic boreholes can be generated in a relatively small model (size will depend on the fracture size) using the orientations of the actual boreholes or a reduced number of boreholes that follow a proportion of the total orientations.

3. Define a range of P_{32} values of interest and generate the line that describes the relationship between P_{32} and P_{10}. Since the relationship is linear, if enough realizations are generated only a point greater than the interval of interest would be needed. Based on the result obtained it is considered that 100 realizations results are appropriate. Note that since the intercept of the linear relationship between the mean and standard deviation of the sampled P_{10} is nonzero, at least two points are needed to calculate the linear relationship between the mean and standard deviation.
4. Calculate P_{10} in actual boreholes and compare this value with the P_{10} sampled in the synthetic boreholes. P_{10} can be obtained as the number of fractures registered per metre during core logging or calculated using televiewer data. Then using the linear relationship between P_{32} and P_{10} (obtained in Step 4) it is possible to convert actual P_{10} to an equivalent P_{32} (Equation 2.11). Using probability functions and interpolations it is possible to estimate the P_{32} variability and probability density for the actual P_{10} (as presented in Figure 4.5).

4.5 Chapter 4 Summary

The main conclusion that can be drawn from this Chapter is that when the boundary effects are mitigated, the relationship between P_{10} and P_{32} is independent of fracture size. Therefore, it is possible to estimate volumetric intensity directly from borehole data. Note that this result should

not be construed to suggest that fracture size is not an important parameter; indeed, fracture size remains a required input for the generation of a DFN model.

The second conclusion is that P_{32} and P_{10} follow a linear relationship, and the results are a further demonstration of the work by Dershowitz (1992) and Elmo (2014). The implication of this is that through simulation it is possible to obtain a relationship between P_{32} and P_{10} even if the borehole data is not oriented. A methodology to estimate P_{32} from P_{10} using DFN modelling was presented, which makes it possible to estimate the P_{32} variability and the probability density for a given P_{10}.

Chapter 5: Volumetric Intensity Derived from Borehole Intensity

5.1 Introduction

It is common practice in the DFN community to calculate linear intensity using drill run lengths and restrict the minimum bias angle to 15° when calculating volumetric intensity (Chilès et al., 2008). This Chapter is dedicated to studying the impact of changing interval length and the minimum bias angle in the calculated P_{32}. Based on the result of the analysis performed, a methodology to calculate P_{32} from borehole intensity is then presented. The main purpose of this methodology is to capture the spatial variation in intensity, while avoiding artificially increasing or decreasing the intensity of the intervals.

5.2 Effect of the Minimum Bias Angle Considered to Estimate P_{32} from P_{10}

Using the DFN model presented in Chapter 4, we calculated the volumetric intensity (P_{32}) from the linear intensity (P_{10}), using the correction proposed by Chilès (2008) presented in Equation 2.4. Note that P_{32} was calculated using the whole well length and the analyses focused on evaluating the effect of the minimum bias angle α (Section 2.3.1) in the estimation of P_{32}. Three cases were considered:

- Minimum α of 15°.
- Minimum α of 5°.
- Minimum α of 1°.

where α represents the acute angle between the scanline and the fracture (see Figure 2.3).

5.2.1 Results of the Effect of the Minimum Bias Angle

Table 5.1 below presents a summary of the ratios between input P_{32} and the P_{32} calculated from linear intensity along the borehole. It can be observed that when limiting the alpha angle to a minimum of 15°, P_{32} is underestimated, especially in boreholes parallel to the fractures (up to 24% for Well 5). On the other hand, when the minimum bias angle decreases, the ratio starts to get closer to one. It is also worth noticing that the standard deviation increases when the minimum angle decreases, suggesting that the dispersion of the data increase for low angles. This effect can be observed in Figure 5.1, in which the input P_{32} is compared with the sampled P_{32} in Well 5, using a minimum angle of 15° and 1°, respectively. Figure 5.1 shows that a good agreement between the input P_{32} and the calculated P_{32} is obtained when using a minimum angle of 1°. These results are in line with Chilès' (2008) recommendations of not discarding data by introducing a minimum bias angle.

The problem with this approach is that is limited to calculate average P_{32} when several boreholes or scanlines with different orientations are available, but it does not allow for calculating the spatial variability of intensity along the wells. Because there is the tendency to calculate linear intensity using run lengths, using smaller angles will result in intervals with high artificial variability in the calculated intensity. Note that the practice of using run lengths as reference intervals has not scientific basis, and is largely dictated by a sort of empirical field practices which are difficult to change. We would suggest to use linear intensity values determined for geotechnical domains, which may include several adjacent core-runs. The effects of using different sampling interval length on the calculated P_{32} will be discussed in Section 5.3.1.

Table 5.1: Ratio Between Input P_{32} and Calculated P_{32} from Borehole Intensity.

Well	Minimum α of 15°		Minimum α of 5°		Minimum α of 1°	
	Average Ratio	SD of Ratio	Average Ratio	SD of Ratio	Average Ratio	SD of Ratio
Well 1	1.12	0.10	1.04	0.11	1.02	0.12
Well 2	1.15	0.11	1.05	0.12	1.02	0.13
Well 3	1.19	0.11	1.07	0.12	1.03	0.14
Well 4	1.14	0.11	1.05	0.12	1.03	0.13
Well 5	1.24	0.13	1.08	0.14	1.03	0.16
Well 6	1.11	0.10	1.04	0.10	1.01	0.11
Well 7	1.11	0.10	1.04	0.10	1.02	0.12
Well 8	1.16	0.12	1.05	0.12	1.02	0.13
Well 9	1.15	0.11	1.05	0.12	1.02	0.13
Well 10	1.13	0.10	1.05	0.11	1.03	0.12
Total	1.15	0.12	1.05	0.12	1.02	0.13

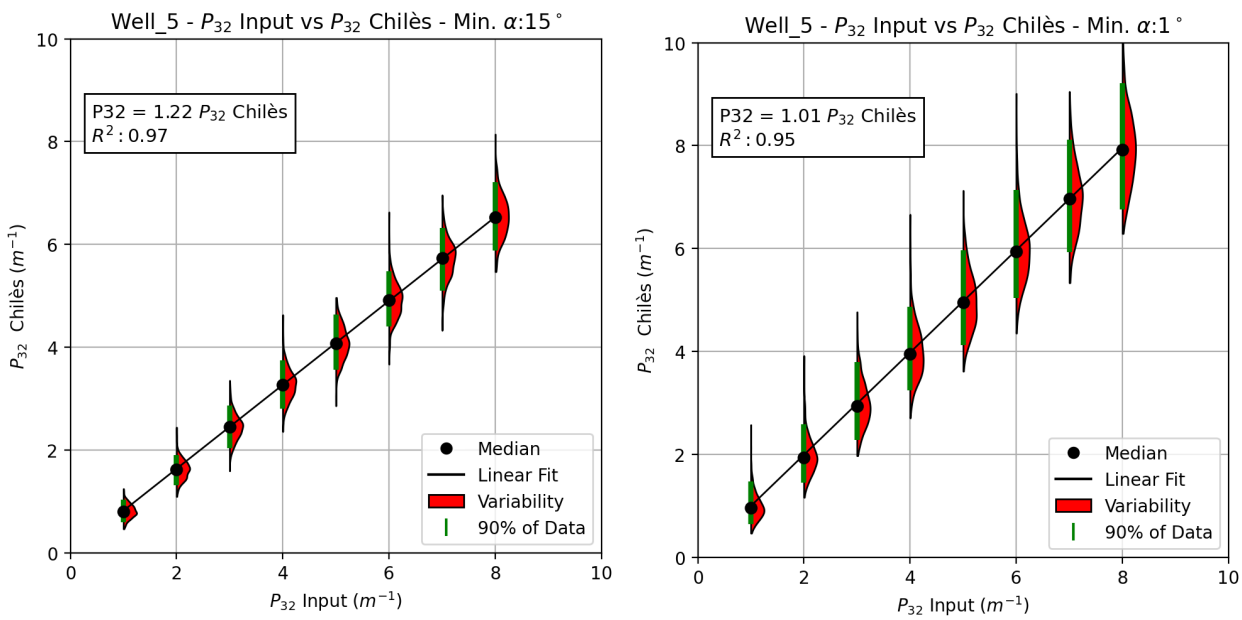

Figure 5.1: Input P_{32} compared to Calculated P_{32} for Well 5. Left Chart: Using a Minimum Angle of 15°. Right Chart: Using a Minimum Angle of 1°.

5.3 Effect of Interval Length in Calculated P_{32} from P_{10}

The effects of varying the interval length on the calculated P_{32} were investigated using simple DFN models with constant fracture orientations. When the fracture orientation and the sampling length are constant, Equation 2.4 can be expressed as:

$$\hat{P}_{32} = \frac{1}{L}\sum_{i=1}^{N}\frac{1}{\sin\alpha} = \frac{N}{L\sin\alpha} = \frac{P_{10}}{\sin\alpha} \qquad \text{Equation 5.1}$$

where α represents the acute angle between the scanline and the fracture (see Figure 2.3).

A volume of interest was defined in a box of 100 m per side, and DFN models were generated using a box size according to the recommendations presented in Chapter 3. DFN models were sampled with a 100 m long vertical well, thus the α angle is equal to the input plunge of the fracture and the results are independent of the fracture trend. Table 5.2 summarizes the properties used in the models to investigate the effects of the interval length in the calculated P_{32}.

Table 5.2: Input Parameter Used in the Models to Investigate the Effects of Interval Length in Calculated P_{32}.

Property	Note
Orientation	Constant Plunge of 90° – 45° – 30° – 15° – 5° – 2 – 1°
Spatial model	Enhanced Baecher with generation locations at fracture centre
Intensity P32 (m^{-1}) values	1 – 2 – 4 – 8
Size: Lognormal Distribution	Radius Mean (Xmean): 2 – 10 – 20 (m) and Standard Deviation (SD) of 40 % of the mean radius size
Fracture Shape	Hexagon with a constant aspect ratio of 1
Number of equiprobable realizations	10 realizations per model (840 realizations in total from the combinations of intensity, size and α)

The well was discretized in regular intervals of 2 m, 5 m, 10 m, 20 m, 50 m, and 100 m. At the same time, boxes centred in each interval, and with the same side length as the intervals were used to calculate the actual P_{32} per interval (sampled P_{32}). The actual P_{32} per interval was then compared with the P_{32} calculated using Equation 5.1, based on the P_{10} values sampled per well interval. Note that for this exercise it was not necessary to estimate the P_{32} correction factor, since the actual P_{32}

in each box was compared with P_{32} calculated in each interval, for the same reason the actual and sample P_{32} values are higher than the input P_{32} values presented in Table 5.2.

5.3.1 Results of the Model to Investigate the Effect of the Interval Length

Figure 5.2 presents the results of the comparison between actual P_{32} and calculated P_{32} for different interval sizes. For small α angles the dispersion increase significantly for small size intervals, with many values out of the graph scale. On the other hand, for 50 m and 100 m intervals, the values tend to follow the line that defines the linear fit of the data. Note that the slope of the line is close to one for all cases, even for those with great dispersion. This effect can be explained since for small α angles the probability to intersect a small interval is low, therefore many of the small intervals present P_{32} values of zero. Contrastingly, the intensity for those intervals that do intersect a fracture is extremely high. Those artificial low and high intensities diverge from the actual intensity, but when they are averaged, they result in P_{32} values close to the actual intensity, as is presented in Table 5.3. This effect was already discussed by (Hekmatnejad et al., 2017), who found that on a composite scale (interval scale), fluctuations in calculated P_{32} are large and there may be a significant deviation between the calculated and the actual value of P_{32}, although in average the values tend to the actual P_{32}.

It can be observed in Table 5.3 that even when the P_{32} calculated in small intervals present a high dispersion, their mean tent to represent the actual P_{32}. This is an interesting result, that suggests that it would be possible to reduce the dispersion by using longer intervals for small α angles and smaller intervals for greater α angles.

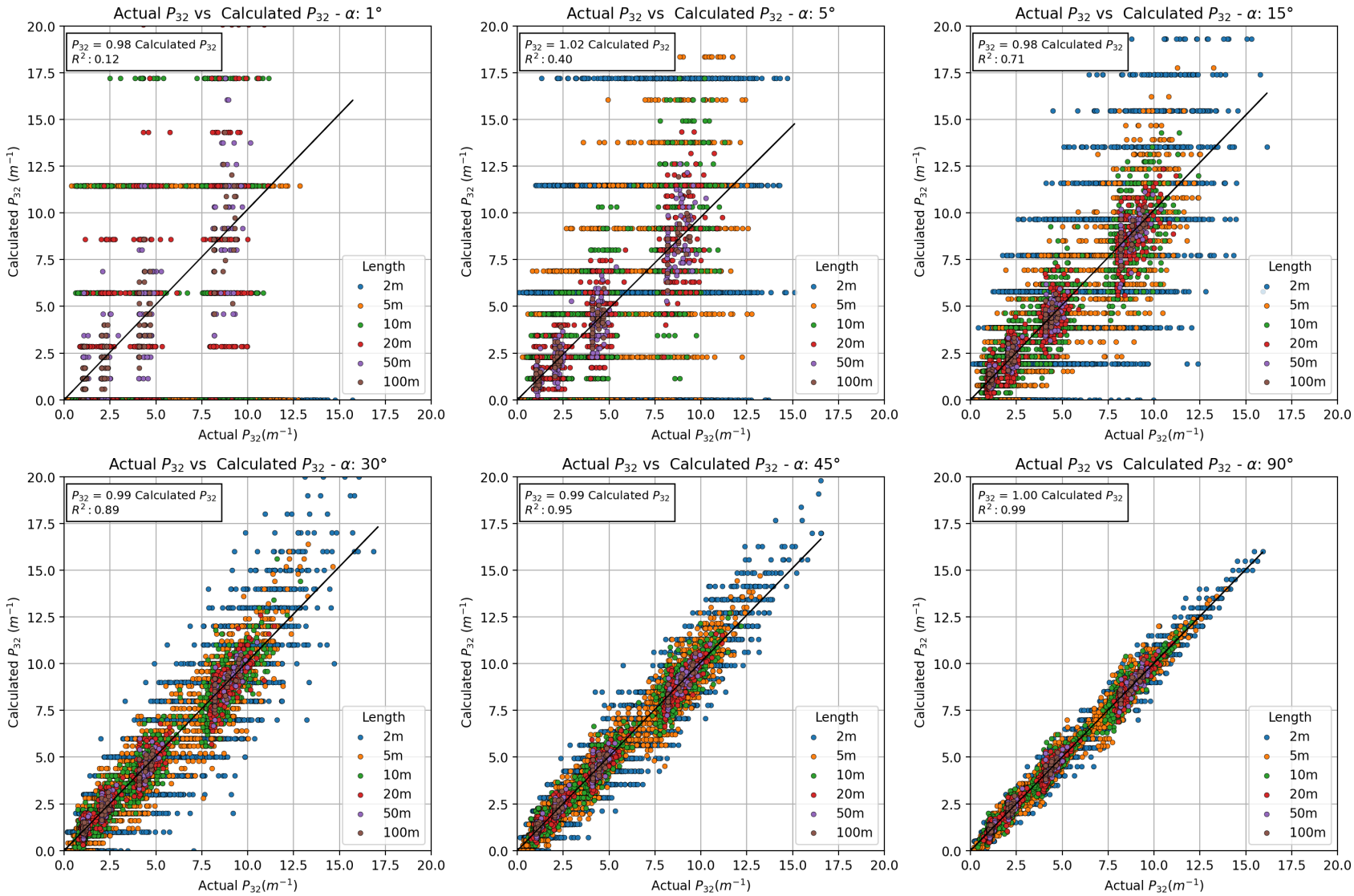

Figure 5.2: Actual P_{32} Compared to Calculated P_{32} Using Different Interval Sizes and α Angles. Black Line Correspond to the Linear Fit of the Data.

Table 5.3: All Cases Combined (α =1,2,5,15,30, 45 and 90°), Using a Minimum α of 1°, Equivalent to a Maximum Factor of 57.3.

Input P_{32} (m^{-1})	Average Actual P_{32} (m^{-1})						Calculated P_{32} (m^{-1})					
	Box Size Per Side						Well interval					
	2m	5m	10m	20m	50m	100m	2m	5m	10m	20m	50m	100m
1	1.2	1.1	1.1	1.1	1.1	1.1	1.2	1.2	1.2	1.2	1.2	1.2
2	2.3	2.3	2.2	2.2	2.2	2.2	2.3	2.3	2.3	2.3	2.3	2.3
4	4.5	4.5	4.4	4.4	4.4	4.4	4.5	4.5	4.5	4.5	4.5	4.5
8	8.9	8.9	8.9	8.8	8.8	8.8	8.9	8.9	8.9	8.9	8.9	8.9
1	1.2	1.1	1.1	1.1	1.1	1.1	1.2	1.2	1.2	1.2	1.2	1.2
2	2.3	2.3	2.2	2.2	2.2	2.2	2.3	2.3	2.3	2.3	2.3	2.3

To investigate the appropriate length to use for each α angle, the maximum calculated P_{32} was plotted for each interval length. Figure 5.3 shows the maximum calculated P_{32} per interval for input intensities of 1 m^{-1} and 8 m^{-1}. The data presented in Figure 5.3 suggests that for α angles greater than 15 °, intervals with lengths ranging from 10 m to 15 m can be used. While for α angles between 2° and 15 °, intervals with a length between 20 to 50 m need to be used, finally for α angles between 1° and 2°, an interval length greater than 50 m is required.

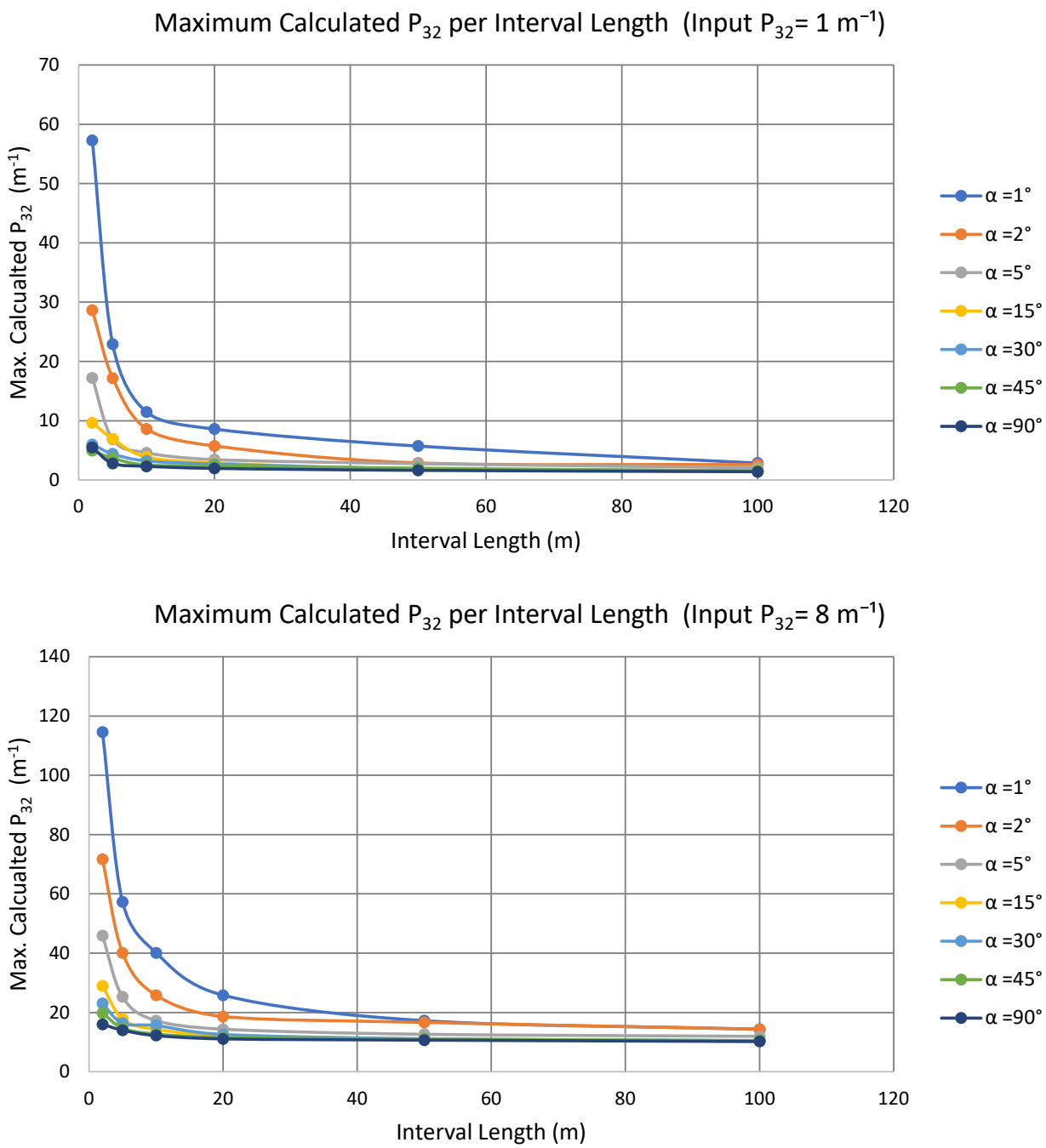

Figure 5.3: Maximum Calculated P_{32} per Interval Length for Input Intensities of 1 m^{-1} and 8 m^{-1}.

5.4 Proposed Methodology to Calculate P_{32} from Borehole Intensity

Based on the analyses performed, a methodology to calculate P_{32} from borehole intensity is proposed. This methodology can be easily implemented using code, and the idea behind this is to allow the calculation of P_{32} in intervals small enough to capture the spatial variation in intensity, but at the same time without artificially increasing or decreasing the intensity of the interval. This is very useful when the interval intensity is used as input in block models, in which artificial changes in intensity may affect the result of the interpolation values in the block model. Block models of P_{32} can be built directly from the borehole composite (borehole interval) data to predict larger supports (blocks), via spatial interpolation or geostatistical techniques (Hekmatnejad et al., 2017).

The following methodology is proposed to calculate P_{32} from borehole intensity:

- Since P_{32} is an additive variable, it is possible to discretize a borehole in different overlapping intervals and calculate P_{32} as the addition of the P_{32} calculated in each interval, as long as the fractures belonging to each interval are not double-counted.
- Based on the previous, it is possible to calculate P_{32} using the correction proposed by Chilès (2008) (Equation 2.4), using regular intervals whose length depends on the magnitude of the acute angle (α) between the scanline and the fracture. Table 5.4 presents the recommended length intervals for each angle.
- Add the P_{32} values calculated using the smallest intervals, this addition corresponds to the total P_{32}.

Note that if only the average intensity is required, it is recommended to calculate P_{32} using the whole length of the borehole or the length within the structural domain of interest. It is still

recommended to limit the minimum α angle to 1°, to avoid extreme high weighting factors or division by zero.

Table 5.4: Recommended Interval Length to Calculate P_{32}.

α Angle (°)	Interval Length to Calculate P_{32}	Notes
$15 \leq \alpha$	10 m to 20 m	Use a length similar to the size of the block model cells.
$2 \leq \alpha < 15$	20 m to 50 m	P_{32} must be calculated within the same Structural Domain
$1 \leq \alpha < 2$	50 m to total borehole length	It can be extended at the full well length. P_{32} must be calculated within the same Structural Domain

5.5 Validation of Proposed Methodology

The proposed methodology was tested using the DFN model and synthetic wells presented in Section 4.2. The interval lengths used, depending on the acute angle between the well and the fracture, are presented in Table 5.5.

Table 5.5: Intervals Used to Test the Methodology Proposed to Calculate P_{32} Depending on α Angle.

α Angle (°)	Interval Length to Calculate P_{32}	Maximum Weighing Factor per Fracture
$15 \leq \alpha$	15 m	3.9
$2 \leq \alpha < 15$	30 m	28.7
$1 \leq \alpha < 2$	90 m (well total length)	57.3

5.5.1 Results Using the Methodology Proposed

Figure 5.4 shows P_{32} values calculated for a range of input P_{32} for each of the synthetic well considered. Independent of the borehole direction, a good agreement is observed between the input P_{32} and the median (Percentile 50%) of calculated P_{32}. Figure 5.5 presents a comparison between the proposed methodology and the P_{32} values calculated in Well 5 using different interval sizes and minimum α angles, while Table 5.6 presents the main finding for each one of the cases analyzed.

As shown in Figure 5.5 and Table 5.6, the methodology herein proposed is the one that provides the best result in terms of a good agreement between input P_{32} and calculated P_{32}, and at the same time maintaining a relatively low variability.

Note that when a minimum angle of 15° is considered the mean P_{32} values calculated are underestimate. This is especially relevant considering that it is common practice to use a minimum angle of 15° (Chilès et al., 2008) to restrict the maximum weighting factor.

An interval of 3 m corresponds to the typical length of a drill run. It is common practice (but not necessarily best practice) to calculate linear intensity on a run basis and then estimate P_{32} using the same length of the run. The analyses performed show that using a length of 3 m, even when restringing the minimum angle to 15 °, produces a high variability on the calculated P_{32}, meaning

that in many cases the calculated P_{32} will be under or overestimated. Note that, in practice, depending on the drilling operation and quality of the rock, the actual drilling run lengths are variable and they may be significantly smaller than 3 m. This means that if P_{32} is calculated using those shorter intervals, the P_{32} variability may be much higher than the one calculated using 3 m intervals. These results agree with the work by Elmo and Stead (2021) and Yang et al. (2020) on the problems of using run lengths to calculate RQD (rock quality designation, Deere, 1967), which is an empirical rock mass quality parameter linked to fracture frequency (i.e., linear intensity).

Table 5.6: Summary of Main Finding for Each One of the Cases Analyzed

Case	Min. α Angle (°)	Interval Length (m)	Main findings
Case 1	1	3	• Linear fit and mean calculated values present a good agreement with input values. • The calculated values present high variability. • Mean values differ from median values (not normally distributed).
Case 2	15	3	• Median P_{32} values calculated are underestimated. • Mean slightly higher than median values. • The calculated values present high variability.
Case 3	1	15	• The linear fit and mean calculated values present a good agreement with the input values. • Mean slightly higher than median values. • The calculated values present high variability.
Case 4	15	15	• Median P_{32} values calculated are underestimated. • The calculated Mean and median values are similar. • Relatively small variability.
Proposed Methodology	Variable as per Table 5.5	Variable as per Table 5.5	• The linear fit and mean calculated values present a good agreement with input values. • The calculated Mean and median values are similar. • Relatively small variability.

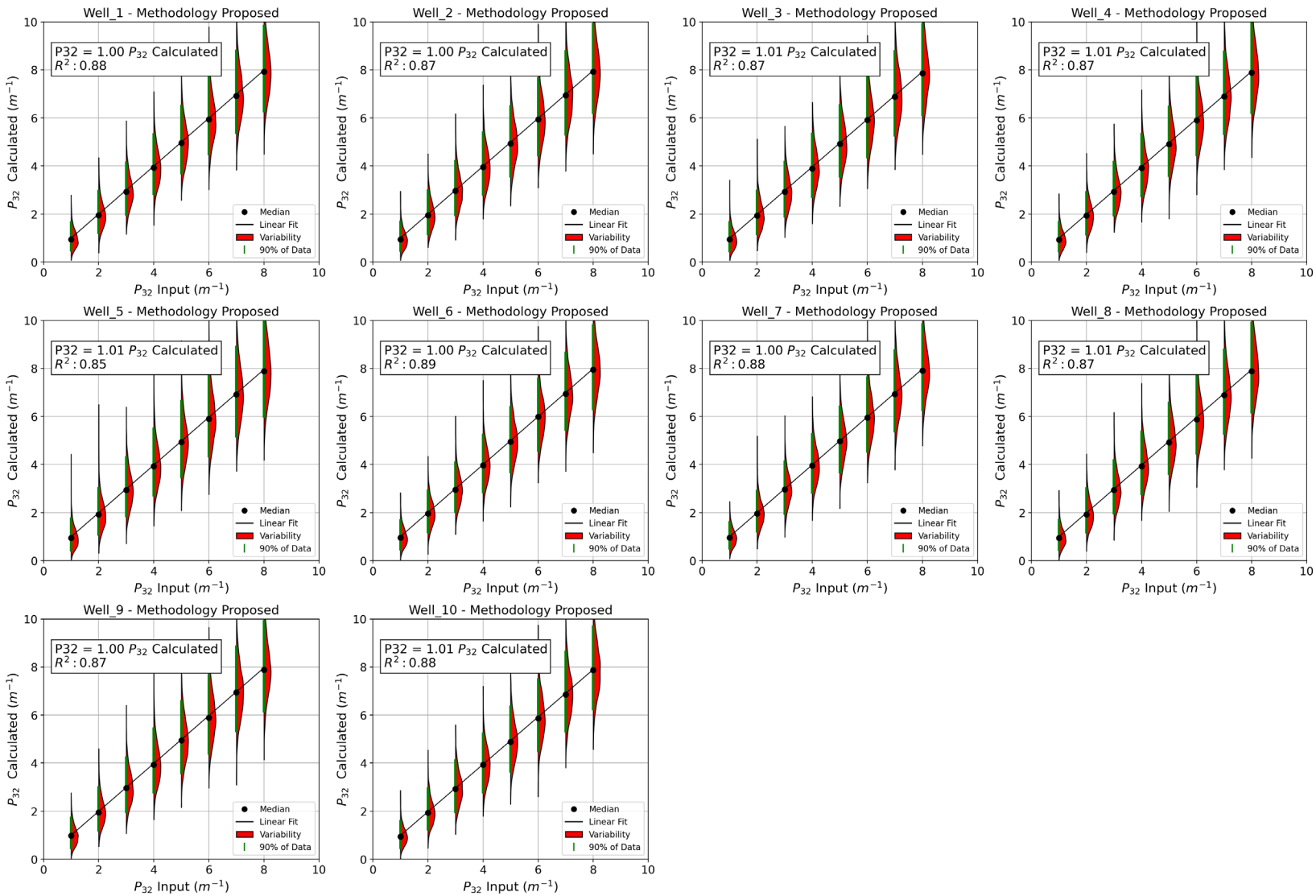

Figure 5.4: P_{32} Calculated per Well Using the Methodology Proposed.

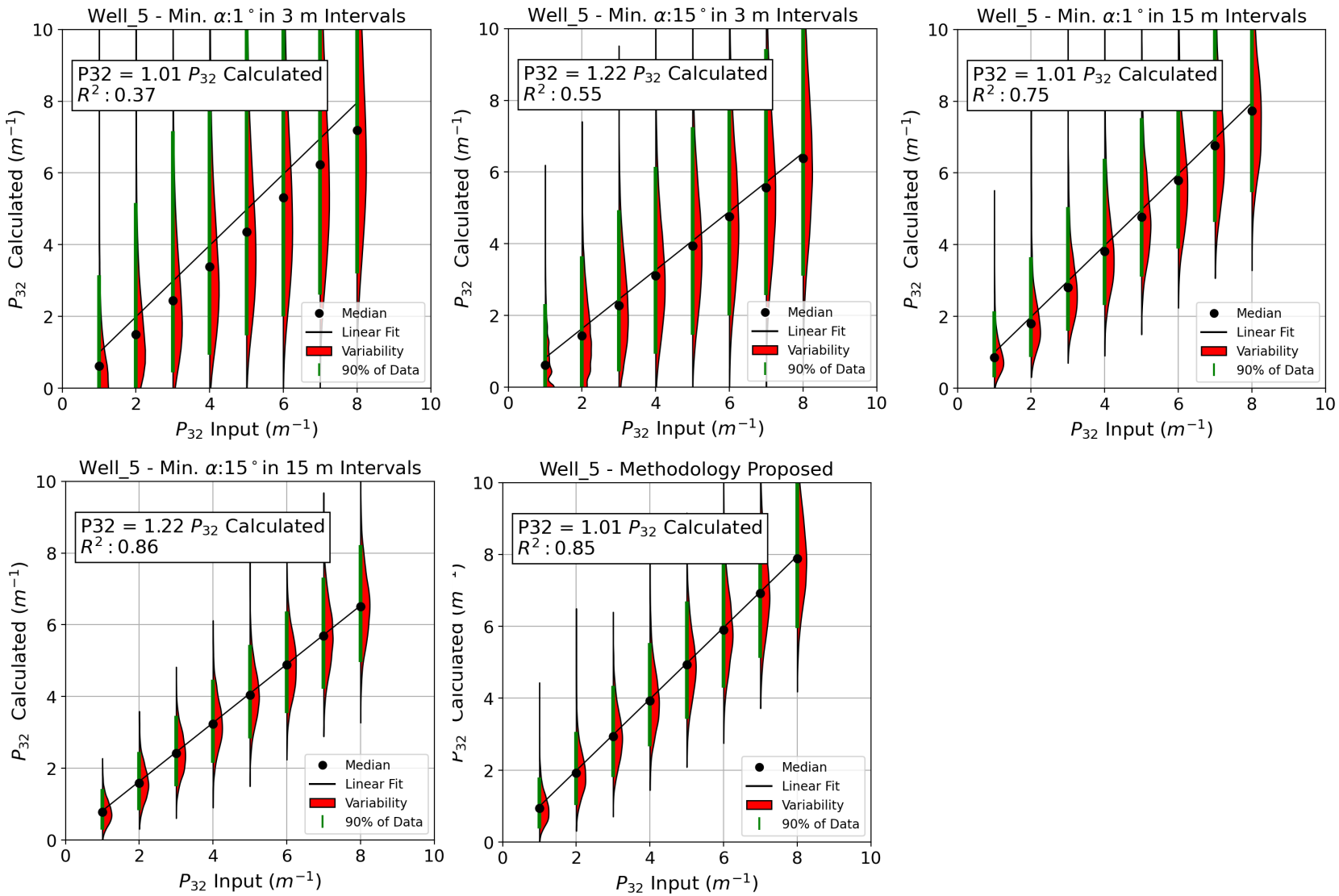

Figure 5.5: P_{32} Values Calculated in Well 5 Using Different Interval Sizes and Minimum α Angles.

As another method of validation, P_{32} values were calculated using a grid with a total volume and location equal to the volume of interest, using cells of 10 m per side. In the cells, P_{32} is calculated as the area of fractures within the grid cell divided by the volume of the grid cell.

Figure 5.6 presents an example of the P_{32} values calculated in the grid for one realization using an input P_{32} of 6 m^{-1} and a mean fracture radius of 20 m, while Figure 5.7 shows a cross-section with a comparison between the grid values and the values calculated in the wells.

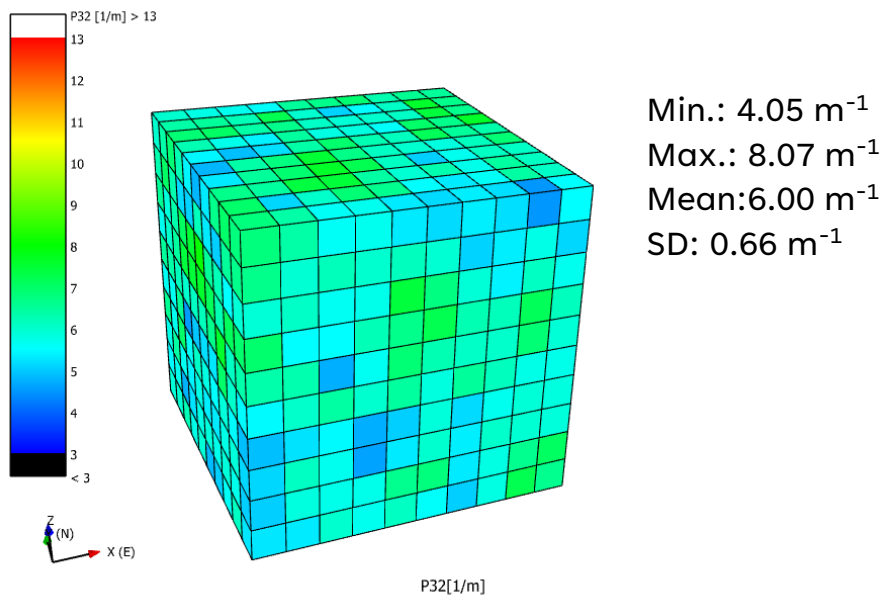

Figure 5.6: P_{32} values calculated in Grid for One Realization Using an Input P_{32} of 6m^{-1} and Mean Fracture Radius of 20 m.

As shown in Figure 5.7, when applied, the proposed methodology captures the spatial variation of P_{32} at the same time a good agreement is obtained between the actual P_{32} (P_{32} values calculates in the grid) and the calculated P_{32} in the wells. On the other hand, when P_{32} is calculated in 3 m intervals, high variability is observed, with values that are artificially low or high and that do not

agree with the actual values calculated on the grid cells. Figure 5.8 presents the result of 100 realizations as cumulative frequency curves of actual P_{32} in the grid cells and the calculated P_{32} in wells. It can be observed, that of the cases analyzed, the methodology proposed is the one that produces the best results, especially when compared with the common practice of limiting the minimum angle to 15° and calculating P_{32} using the drill run length (3 m).

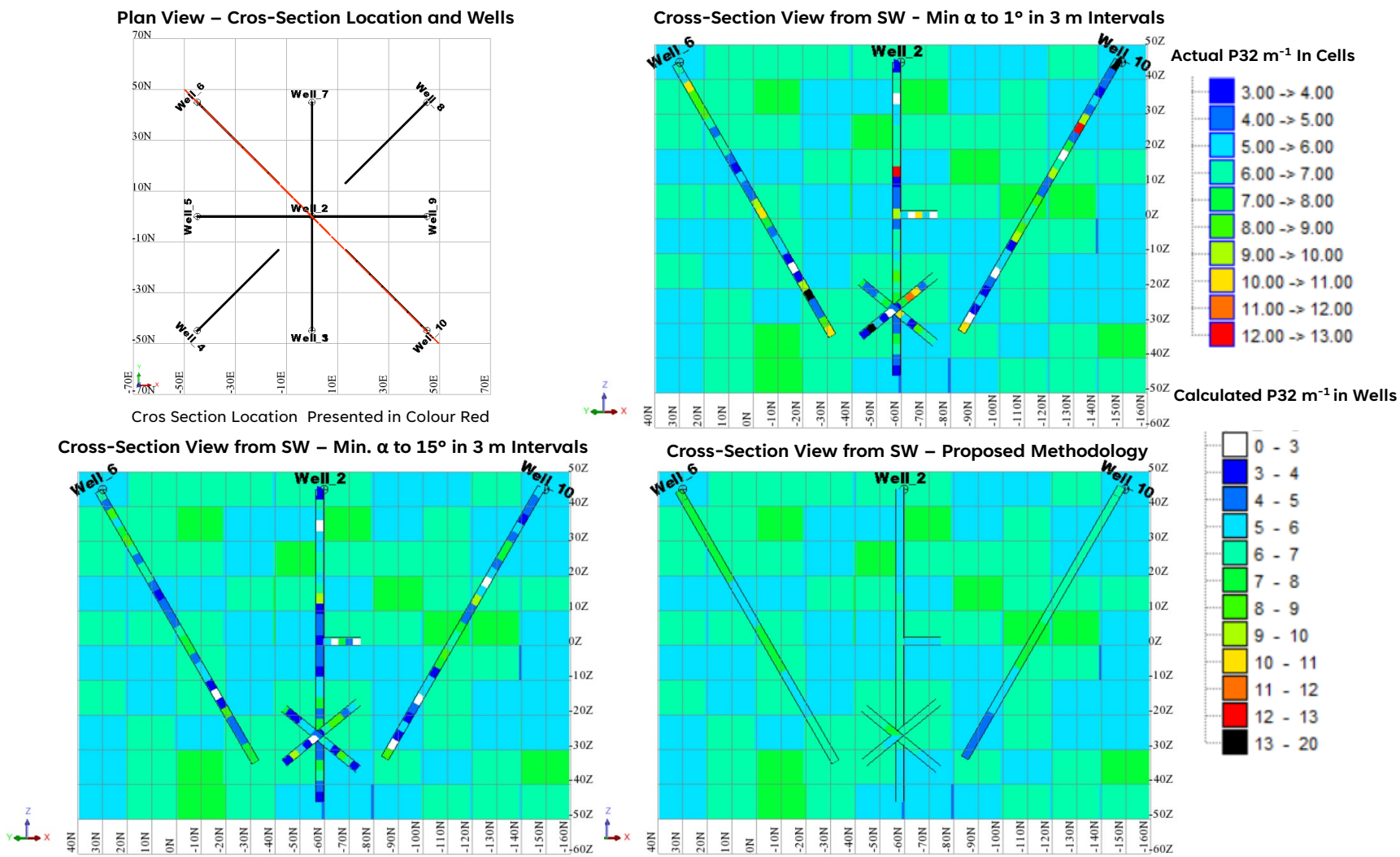

Figure 5.7: P_{32} Values Calculated in Grid for One Realization- Cross-Sections and Comparison with Calculated P_{32} Values in Wells.

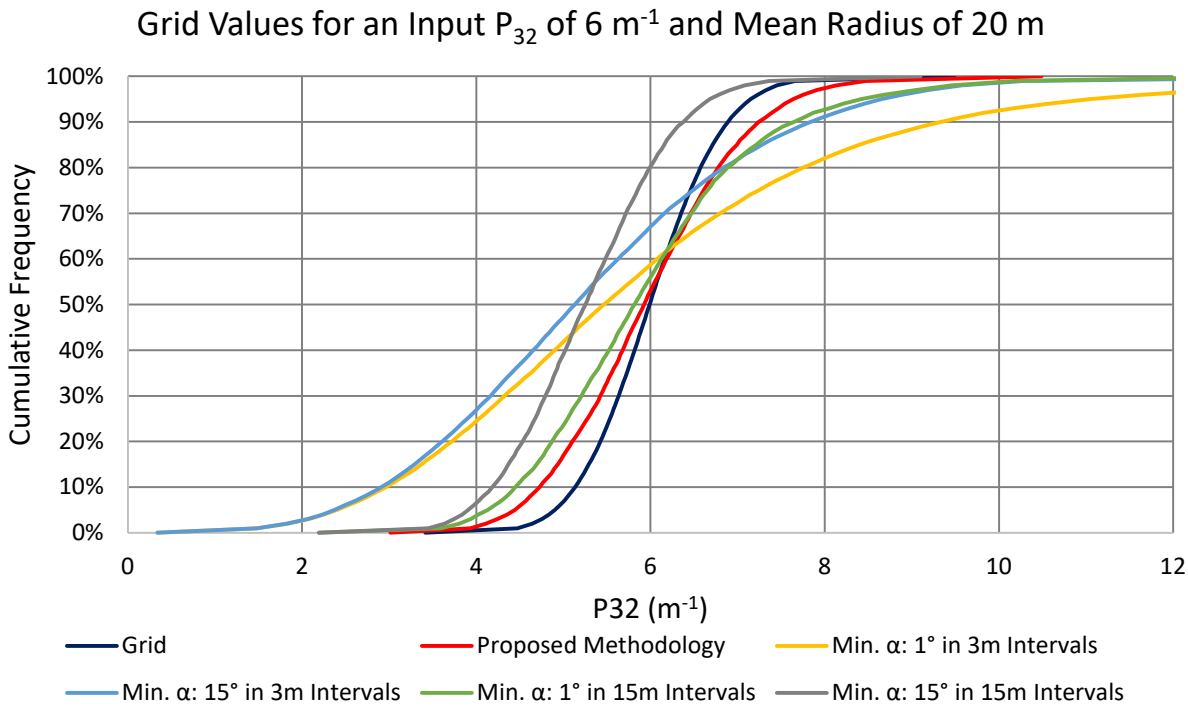

Figure 5.8: Cumulative Frequency Curves for Actual P_{32} in Grid Cells and Calculated P_{32} in Wells for an Input P_{32} of 6 m^{-1} and a Mean Fracture Radius of 20 m. Values Presented Correspond to the Result of 100 Realizations.

5.6 Chapter 5 Summary

This Chapter was dedicated to the study of the effects of the minimum bias angle and the interval length on P_{32} values calculated from linear intensity. The result of the analysis performed showed that when using a minimum angle of 15°, corresponding to the value commonly used by the DFN community, the mean P_{32} values calculated are underestimated. On the other hand, when the drill run lengths are used to calculate P_{32}, an artificial variability in the data is introduced. Based on the previous observations, a methodology to calculate P_{32} using variable lengths, depending on the angle between the fractures and the sampling line (borehole) was proposed. The main purpose of this methodology is to capture the spatial variation in intensity and at the same time avoid

increasing or decreasing artificially the intensity of the intervals. This is very useful when the interval intensity is used as input for interpolating P_{32} values in block models.

The proposed methodology was compared with current practices of constraining the minimum bias angle to 15° and calculating P_{32} using small intervals (drill run lengths), showing that when the proposed methodology is used a better agreement is observed between actual and calculated P_{32}.

Chapter 6: Conclusion

6.1 Research Summary

A main component of the rock mass characterization is the characterization of discontinuities, which play a major role in the mechanical and hydraulic properties of rock masses. This thesis focused on volumetric fracture intensity, which is one of the key properties of fracture characterization for DFN modelling and that is not possible to measure directly on rock masses.

The problem of estimating volumetric fracture intensity from information observed along boreholes was addressed by generating a series of DFN models and then comparing the volumetric intensity of those models with the volumetric intensity calculated from borehole intensity, using a methodology based on the methodology proposed by Chilès (2008).

During the development of this research the following activities were performed:

- The boundary effects on DFN models were investigated and a methodology to mitigate the boundary effects on intensity was proposed.
- The relationship between borehole fracture intensity and volumetric fracture intensity was investigated and a methodology to quantify the reliability of the volumetric fracture intensity derived from borehole fracture intensity was proposed.
- A methodology to calculate P_{32} from borehole P_{10} was proposed. This methodology allows capturing the spatial variation in intensity while at the same time avoiding increasing or decreasing artificially P_{32} calculated in borehole intervals. This is very useful when the interval intensity is used as input for block modelling of P_{32} values.

6.2 Main Finding and Conclusions

The main findings of this research can be summarized as follows:

- The analyses performed confirmed that DFN models do present boundary effects on intensity, something that was already discussed by Priest (1993), but that it is often disregarded when building DFN models.
- The boundary effect on the fracture intensity and other derived analyses may be considerable. It is necessary the evaluation and quantification of the boundary effects before considering the application of any DFN.
- It is possible to minimize the boundary effect for DFN models when the generation box is defined as a function of the fracture size and the dimensions of the volume of interest. A correction factor for the input P_{32} can be defined to correct the intensity generated in the volume of interest. This factor will be dependent on the size of the volume of interest, the size of the generation box, the fracture size distribution, and the fracture orientations.
- The analysis showed that when the boundary effects are mitigated, the relationship between P_{10} and P_{32} is linear and independent of the fracture size. This implies that it is possible to estimate volumetric intensity directly from borehole data. Note that this result should not be construed to suggest that fracture size is not an important parameter; indeed, fracture size remains a required input for the generation of a DFN model.
- Since the rock mass behaviour is controlled by fracture connectivity and intensity is independent of the fracture size, it demonstrates that P_{32} is not the ideal parameter to define by itself, rock strength or rock mass quality.
- The analysis showed that using simulation it is possible to quantify the variability and distribution of the volumetric intensity for a given linear intensity. Note that more than a

unique P_{32} value can be obtained for a given P_{10} value, but whit this methodology is possible to quantify the probability to obtain a certain P_{32} for a given P_{10}.

- The general practice of constraining the minimum bias angle to 15° and calculating P_{32} using small intervals (drill run lengths), results in underestimation and high variability of the calculated P_{32}. When using the methodology proposed by Chilès (2008) to calculate P_{32}, the size of the interval has a great impact on the variability of the calculated P_{32}. Using small intervals will increase artificially the variability of the calculated P_{32}, even when the average P_{32} tends to be close to the actual P_{32}. On the other hand, when limiting the minimum angle between the fracture and the borehole to a minimum of 15°, the mean calculate P_{32} values are underestimated.
- The proposed methodology to calculate P_{32} using variable lengths, depending on the angle between the fractures and the borehole, allows to capture the spatial variation in intensity and at the same time avoid increasing or decreasing artificially the intensity of the intervals. This is very useful when the interval intensity is used as input for interpolating P_{32} values in block models.
- When only the average volumetric intensity is required, it is recommended to calculate P_{32} using the total length of the borehole or the length within the structural domain of interest. In this case, it is recommended to limit the minimum α angle to 1°, to avoid extreme high weighting factors or division by zero.

6.3 Limitations and Assumptions

The research described previously is subject to the following limitations and assumptions:

- The main limitation of this study is that the analyzes presented are purely simulated and have not yet been applied to real data. However, we need to consider that is impossible to measure P_{32} directly in the field, and therefore we will always have to rely on simulations to determine P_{32}. The concept of validating modelling results with field data does not apply to P_{32} values since it is not possible to directly compare calculated P_{32} with the actual P_{32} of the rock mass (unknown).
- All fractures have been assumed planar and extremely thin. Although fractures in nature can be curved and present thickness, it is common practice to assume that discontinuities are planar (Warburton, 1988; Zhang and Einstein, 1998).
- It was assumed that the fractures present a hexagonal shape with a constant aspect ratio of 1. Although the assumption that fractures are equidimensional is commonly used, some investigators indicate that fractures are in reality not equidimensional (Zhang and Einstein, 1998).
- It was assumed in the models that fractures are randomly and independently distributed in space. In reality, fracture intensity may be depended on geological features, for example, a common geological observation is that fracture intensity is controlled by the distance to major faults (McCaffrey et al., 2003).
- The analysis performed assumed that all fractures intersected by the synthetic wells are identified. In practice, there are biases when gathering fracture intensity from boreholes. For example, besides the orientation bias, it is common that during borehole logging not all-natural discontinuities are counted and some artificial fractures (e.g., mechanical breaks

generated during drilling and handling of the core samples) are counted as natural fractures. Even if the fracture intensity is calculated from televiewer data (i.e., data obtained with equipment that captures images of the borehole wall), the quality of the data depends on the quality of the images and the interpretation performed of each discontinuity.

- The methodology proposed to avoid boundary effects may be impracticable when the fractures are too big. For big fractures it would be necessary to generate an extremely big generation box, that may require extensive computation time.

6.4 Recommendations for Future Works

The following recommendations for future works are made:

- We would recommend to further study the application of the proposed methodology to calculate P_{32} using variable lengths depending on the angle between the fractures and the borehole, to an actual project.
- We would recommend to further quantify the error of P_{32} values interpolated in a block model from borehole data, and compare the results obtained using the proposed methodology with the results obtained using the common practice of calculating P_{32} using drill run lengths and limiting the minimum angle between the borehole and the fracture to 15°. This can be done by generating a DFN model of known P_{32}, then the actual P_{32} can be estimated in each block, and those values can be compared to the interpolated values from the borehole intervals. This will allow quantifying the benefits of using the methodology proposed in block modelling of P_{32}.
- We would recommend to further test the validity of the methodology proposed to calculate P_{32}, using a geocellular generated DFN model, in which the intensity of the DFN in each

cell (block) can vary. Then compare the sampled volumetric intensity of each cell with the volumetric intensity calculated from the borehole intersections with the DFN. This will allow quantifying the ability of the proposed methodology to capture the spatial variation in intensity.

Bibliography

Baecher, G.B., Lanney, N.A. 1978. and H.H. Einstein. Statistical Description of Rock Properties and Sampling. Proceedings of the 18th U.S. Symposium on Rock Mechanics, 5C1-8.

A. Brzovic, S. Rogers, G. Webb, J. P. Hurtado, N. Marin, P. Schachter, J. Alvarez and K. Baraona. 2015. Discrete fracture network modelling to quantify rock mass pre-conditioning at the El Teniente Mine, Chile, Mining Technology, 124:3, 163-177, DOI: 10.1179/1743286315Y.0000000019.

Chilès, J.P., Wackernagel, H., Beucher, H., Lantuéjoul, C. and Elion, P. 2008. Estimating fracture density from a linear or areal survey. In: Ortiz, J.M., Emery, X. (Eds.), Proceedings of the Eighth International Geostatistics Congress. Gecamin Ltda, Santiago, pp. 535–544.

Deere, D.U., Hendron, A.J., Patton, F.D. and Cording, E.J. 1967. Design of surface and near surface construction in rock. In Failure and breakage of rock, proc. 8th U.S. symp. rock mech., (ed. C. Fairhurst), 237-302. New York: Soc. Min. Engrs, Am. Inst. Min. Metall. Petrolm Engrs.

Dershowitz, W.S. 1984. Rock joint systems. PhD. Thesis. MIT, Cambridge, MA.

Dershowitz, W.S., Einstein, H.H. 1988. Characterizing rock joint geometry with joint system models. Rock Mech Rock Engng 21, 21–51. https://doi.org/10.1007/BF01019674.

Dershowitz, W.S. and H.H. Herda. 1992. Interpretation of fracture spacing and intensity. Proc. 33rd U.S. Rock Mech. Symp., Santa Fe, NM.

Dershowitz, W. S., Finnila, A., Rogers, S., Hamdi, P., and K. M. Moffitt. 2017. "Step Path Rock Bridge Percentage for Analysis of Slope Stability." Paper presented at the 51st U.S. Rock Mechanics/Geomechanics Symposium, San Francisco, California, USA, June 2017.

Elmo, D. Liu, Y., and Rogers, S. 2014. Principles of discrete fracture network modelling for geotechnical applications. International Discrete Fracture Networking Conference. DFNE 2014 - 238.

Elmo, D and Stead, D. 2010. An integrated numerical modelling—discrete fracture network approach applied to the characterisation of rock mass strength of naturally fractured pillars. Rock Mech Rock Eng 43(1):3–19.

Elmo, D. and Stead, D. 2021. The concept of representative elementary length (REL) as an effective tool to study scale effects in rock engineering problems. Boletín Geológico y Minero, 131 (3): 355-362 ISSN: 0366 -0176. 10.21701/bolgeomin.131.3.001.

Elmo, D., Stead, D. and Rogers, S. 2008. Quantitative analysis of fractured rock masses using a discrete fracture network approach: Characterisation of natural fragmentation and implications for current rock mass classification systems. 5th International Conference and Exhibition on Mass Mining.

Golder Associates. 2021a. FracMan Version 8.1. FracMan Technology Group. https://www.golder.com/fracman/.

Golder Associates. 2021b. Golder Associates (UK) Ltd. FracMan 8.0 Manual. February 2021.

Hekmatnejad, A., Emery, X., Brzovic, A., Schachter, P. and Vallejos, J.A. 2017. Spatial modeling of discontinuity intensity from borehole observations at El Teniente mine, Chile. Engineering Geology, 228, 97-106.

Junkin, W. R., Ben-Awuah, E. and L. Fava. 2019. "DFN Variability Analysis Through Voxelization." Paper presented at the 53rd U.S. Rock Mechanics/Geomechanics Symposium, New York City, New York, June 2019.

Kiràly, L. 1969. Statistical analysis of fractures (Orientation and density). Geol Rundsch 59, 125–151 (1969). https://doi.org/10.1007/BF01824947.

Mauldon, M., and Mauldon, J. G. 1997. Fracture sampling on a cylinder: From scanlines to boreholes and tunnels. Rock Mechanics and Rock Engineering, 30(3), 129-144. doi:https://doi.org/10.1007/BF01047389.

Mauldon, M. 1998. Estimating mean fracture trace length and density from observations in convex windows. Rock Mech. Rock Engng. Vol. 31. pp. 201-216.

McCaffrey, K.J.W, Sleight, J.M, Pugliese, S and Holdsworth, R.E. 2003. Fracture formation and evolution in crystalline rocks: Insights from attribute analysis. Geological Society, London, Special Publications. 214. pp. 109-124. 10.1144. doi:10.1016/0148-9062(76)90818-4

Munkhchuluun, M., Elmo, D., Nadolski, S., and B. Klein. 2017. "Characterization of Rock Mass Fragmentation for Cave Mining." Paper presented at the 51st U.S. Rock echanics/Geomechanics Symposium, San Francisco, California, USA, June 2017.

Priest, S.D. 1993. Discontinuity Analysis for Rock Engineering. Chapman and Hall, London. Springer Netherlands.

Rocsience. 2022. Dip User Guide. Retrieved from https://www.rocscience.com/help/dips/documentation/stereonet-plots/terzaghi-weighting

Rogers S, Elmo D, Beddoes R and Dershowitz B (2009) Mine scale DFN modelling and rapid upscaling in geomechanical simulations of large open pits. In: International symposium on rock slope stability.

Rogers, S., Elmo, D., Webb, G., and Catalan, A. 2015. Volumetric Fracture Intensity Measurement for Improved Rock Mass Characterisation and Fragmentation Assessment in Block Caving

Operations. Rock Mech Rock Eng 48, 633–649 (2015). https://doi.org/10.1007/s00603-014-0592-y

Rogers, S. F., Elmo, D., Webb, G. and C. Guajardo. 2016. DFN Modelling of Major Structural Instabilities in a Large Open Pit for End of Life Planning Purposes. Paper presented at the 50th U.S. Rock Mechanics/Geomechanics Symposium, Houston, Texas, June 2016.

Samaniego J.A and Priest S.D. 1984. The prediction of water flows through discontinuity networks into underground excavation. Design and Performance of Underground Excavations: ISRM Symposium, (pp. 157-164). Cambridge, U.K.

Terzaghi, R. 1965. Sources of error in joint surveys, Geotechnique, vol. 15, no. 3, pp. 287-303.

Wang, X. and Mauldon, M. 2006. Proportional errors of hte Terzaghi correction factor. Golden Rocks 2006, The 41st US Symposium on Rock Mechanics (USRMS). Golden, CO.

Wang, X. 2005. Stereological interpretation of rock fracture traces on borehole walls and other cylindrical surfaces (Order No. 3241181). Available from ProQuest Dissertations & Theses Global. (305381859).

P.M. Warburton. 1988. A stereological interpretation of joint trace data. International Journal of Rock Mechanics and Mining Sciences & Geomechanics Abstracts, 17(4), 181-190. Retrieved from https://doi.org/10.1016/0148-9062(80)91084-0.

Yang B., D. Elmo and D. Stead. 2020. Questioning the use of RQD in rock engineering and its implications for future rock slope design. In: Proc. 52nd Int. Symposium on Rock Mechanics, Golden, Colorado, June, 2020. #1404.

Yow JL and Yow JL. 1987. Blind zones in the acquisition of discontinuity orientation data. International journal of rock mechanics and mining sciences & geomechanics abstracts. 10/1987;24(5):317-318. doi: 10.1016/0148-9062(87)90868-0.

Zhang, L. and Einstein, H. 1998. Estimating the Mean Trace Length of Rock Discontinuities. Rock Mech Rock Engng vol. 31, pp. 217–235 (1998). https://doi.org/10.1007/s006030050022

Zhang, L. and Einstein, H. 2000. Estimating the intensity of rock discontinuities, International Journal of Rock Mechanics and Mining Sciences, vol. 37, no. 5, pp. 819-837. ISSN 1365-1609, https://doi.org/10.1016/S1365-1609(00)00022-8.